Rational design of polysorbate 80 stabilized human serum albumin nanoparticles tailored for high drug loading and entrapment of Irinotecan

NeetikaTaneja[a] and Kamalinder K. Singh [b*]

[a]*C. U. Shah College of Pharmacy, S.N. D. T. Women's University, Santacruz (W), Mumbai 400049, India*
[b]*School of Pharmacy and Biomedical Sciences, University of Central Lancashire, Preston, PR1 2HE, United Kingdom*

[*]To whom correspondence should be addressed:

Kamalinder K. Singh
School of Pharmacy and Biomedical Sciences,
University of Central Lancashire,
Preston, PR1 2HE, United Kingdom
Email: ksingh1@uclan.ac.uk; profkksingh@gmail.com

Abstract

Human serum albumin (HSA) nanoparticles are considered to be versatile carrier of anticancer agents in efficiently delivering the drug to the tumor site without causing any toxicity. The aim of the study was to develop stable HSA nanoparticles (NPs) of drug irinotecan (Iro) having slightly water solubility and moderate HSA binding. A novel strategy of employing a hydrophilic non-ionic surfactant polysorbate 80 which forms protein-polysorbate 80 complex with increased affinity and improvement in Iro-HSA binding has been used to maximize the loading and entrapment efficiency of Iro in HSA-NPs. Bespoke nanoparticles with entrapment efficiency (79.09%) and drug loading of 9.62% could be achieved with spherical shape and particle size of 77.38 nm, 0.290 polydispersity index and -23.7 mv zeta potential. The drug entrapment in nanoparticles was confirmed by Differential Scanning Calorimeter, Fourier Transformation Infrared Spectroscopy and Fluorescence spectroscopy. *In-vitro* release of Iro from nanoparticles showed biphasic-release with initial burst followed by prolonged release upto 24h. The short-term stability investigation of nanodispersion showed no significant changes in physicochemical properties of nanoparticles. Long-term studies on freeze-dried Iro-HSA-NPs indicated good stability of nanoparticles up to 12 months. This is the first report for efficient fabrication of Iro delivery system based on HSA nanoparticles.

Keywords: Human serum albumin, nanoparticles, Irinotecan, polysorbate 80, desolvation, high pressure homogenization, response surface methodology, factorial design, stability studies

1. Introduction

Nanoparticles (NPs) are solid or liquid colloidal particles ranging in size from 10 to1000 nm and can be used as drug-carrier platforms (Singh and Lillard, 2009). The most recent development in designing drug delivery system has been focused upon the protein-based nanomedicine, due to their biocompatibility and biodegradability coupled with low toxicity (MaHam et al., 2009). Human serum albumin (HSA), a multifunctional protein for drug delivery has drawn considerable attention in pharmaceutical field in view of its non-toxic, non-immunogenic, biocompatible and biodegradable properties (Sleep, 2015). It also has multiple binding sites, which can act as a carrier for the various drugs. As compared to other NPs made from synthetic polymer, HSA NPs are well tolerated *in vivo* without any side effects, which is supported by the findings of several clinical studies on commercial HSA based NPs such as Albunex® (Barnhart et al., 1990) and Abraxane® (Green et al., 2006). In addition HSA can be preferentially taken up by tumor through well known gp60 pathway, making it an attractive carrier for the delivery of anticancer drugs (Kratz, 2008). Thus, HSA NPs represent a promising strategy for targeted delivery of anticancer drugs to tumor cells by enhancing the drug bioavailability and distribution, diminishing their toxicity and reducing the body's response towards drug resistance (Sheng et al., 2014).

Irinotecan (Iro) an anticancer agent, inhibits topoisomerase I involved in DNA replication (Fuchs et al., 2006) is the first line treatment of metastatic colorectal cancer (Douillard et al., 2000; Sobrero et al., 2008). But unfortunately, Camptosar® the commercial injection of Iro apart from causing irritation of vein and damage to tissues near to administration site causes various gastrointestinal side effects including severe nausea, vomiting and diarrhea. It also results in reduction in the number of white and red blood cells (Hardman et al., 1999). This creates the need to develop an alternative safer drug delivery system that can target the tumor site and

overcome the side effects of the drug due to its non-specific distribution.Various drug delivery systems based on novel polymers are being developed for the safe delievery of the drug (De et al., 2009; Zhu et al., 2013) lipid (Waterhouse et al., 2014), magnetic (Tamyurek et al., 2015), PLGA (Valencia et al., 2013) and chitosan (Guo et al., 2013) carriers also have been investigated for nanoparticulate delivery of Iro. Recently, the US FDA (United States Food And Drug Administration) approved an Iro liposome injection,Onivyde® to treat patients with advanced metastatic pancreatic cancer (Passero Jr et al., 2016). However to best of our knowledge there is no report on Iro deliverysystem based on HSA NPs.

HSA NPs can be prepared by various methods including desolvation (Weber et al., 2000), emulsification (Yadav and Vadali, 2008), thermal gelation (Yu et al., 2006), nanospray drying (Lee et al., 2011), nanoparticle albumin bound (NAB)-technology (Cortes and Saura, 2010) and self-assembly (Desai, 2007). Among all these methods, desolvation is most commonly used method because of high reproducibility and the production of NPs with more controlled drug release properties (Langer et al., 2003). Water-soluble drugs such as doxorubicin (Dreis et al., 2007), ciprofloxacin (Kumar and Jain, 2007), imatinib (Kamali et al., 2015) and 5-fluorouracil (Maghsoudi et al., 2008) have been efficiently loaded in albumin NPs by desolvation technique. However, it is challenging to prepare HSA NPs with sufficient drug loading and entrapment efficiency, especially for drugs having limited solubility and poor drug binding. Iro being moderately water soluble (Ci et al., 2014) and average albumin binding affinity (30-60%) poses such obstacles (Combes et al., 2000).

The present study reports a new strategy of employing a hydrophilic non-ionic surfactant polysorbate 80 during drug HSA incubation to maximize the loading and entrapment efficiency of Iro in HSA-NPs. Polysorbate 80, a approved safe non ionic surfactant was explored in order to prepare stable NPs with high loading of drug. When polysorbate 80 is added to aqueous solution of protein, surfactant-protein complexation occurs (Delgado-Magnero et al., 2014) leading to increased affinity for Iro and improvement in Iro-HSA binding. As Iro has slight water solubility (25mg/mL) and limited albumin binding affinity, it can be trapped inside clusters of polysorbate

80 formed by binding to non-specific surface regions on albumin. This approach was used to improve the binding of Iro to HSA with enhanced drug entrapment and loading in NPs. To achieve tunable NPs, various factors affecting the process of preparation of HSA NPs and material attributes of the formulation were identified using Ishikawa diagram and ranked for probability of risk from low to high using risk estimation matrix (REM). The critical factors affecting the entrapment of drug were further optimized by 3^2 factorial design which is a widely used approach for optimizing systems that depend on factors (dos Santos et al., 2005). The resultant bespoke Iro-HSA-NPs has been extensively characterized by dynamic light scattering (DLS), field emission surface electron microscopy (FESEM), Fourier transformation infrared spectroscopy (FTIR), differential scanning calorimeter (DSC) and fluorescence spectroscopy. The entrapment efficiency, drug loading and *in vitro* release of drug from NPs were also determined. Industrial manufacturing and commercialization is often governed by the stability of the product. The developed NPs were therefore studied for short and long term stability over two-year period.

Material and methods

2.1. Material

Irinotecan hydrochloride trihydrate was obtained as a gift sample from Khandelwal Laboratories Pvt.Ltd, Mumbai, India. Human Serum albumin (Alburel 20%) was purchased from Reliance Life Sciences, Mumbai, India. Polysorbate 80 and absolute ethanol was obtained from S.D Fine Chemicals Ltd., Mumbai, India. Trehalose and mannitol was gift sample from Signet, Mumbai, India.

2.2. Fluorescence quenching Study

Fluorescence spectroscopy is the most common technique used to study the interaction between drug and protein (Anand and Mukherjee, 2013). Fluorescence spectra were recorded with Perkin Elmer LS-55 fluorescence spectrometer,USA. Emission spectra were acquired with an excitation wavelength of 280 nm and emission range of 290–400nm. Both the excitation and emission slit widths were kept at 5nm each.The quenching experiment was carried out by adding 20-400µg of Iro in 1mL of HSA solution (0.1mg/mL) and fluorescence was measured in 1 cm path length

quartz cuvette. Fluorescence intensities at 340 nm were recordedas a function of Iro concentration. Further, binding parameters were obtained using Stern–Volmer equation (Samant et al., 2014):

$$F0/F = 1 + kq \cdot \tau 0 . [Q] = 1 + Ksv[Q] \quad \text{.....(1)}$$

where, F0 and F are fluorescence intensities of HSA in the absence and presence of Iro, respectively, Ksv is the Stern-Volmer quenching constant, [Q] is the concentration of Iro, kq is the bimolecular quenching constant, and τ_0 is the lifetime of the fluorophore.

In another experiment, to understand the individual effect of polysorbate 80 and Iro on fluorescence at the equivalent concentrations used during the preparation of HSA NPs, HSA solution was added with polysorbate 80 (50 fold molar excess) and Iro (0.25µM). Fluorescence emission spectrum was recorded from 280nm-500nm following excitation at 280nm with the slit width of 5 nm. Moreover, spectrum was also recorded when both polysorbate 80 and Iro were added simultaneously to HSA.

2.3. Preparation of human serum albumin nanoparticles of irinotecan (Iro-HSA-NPs)

Iro-HSA-NPs were prepared by desolvation technique according to the method described by Weber et al (Weber et al., 2000) with some significant modifications. For a 100 mL batch, 15 mL of 20% w/v HSA in double distilled water was added to polysorbate 80 (3%w/v) followed by incubation with 100 mg of Iro for 3 hours. After incubation, the resultant solution was desolvated by ethanol at the addition rate of 1mL/min under stirring at constant speed of 500 rpm till the turbidity appeared. After desolvation, ethanol was evaporated and NPs were cross-linked by heating at 60^0C and homogenized in a high-pressure homogenizer (GEA NiroSoavi, Panda Plus, Italy) with attached water circulation pump (Lab Companion, Biotechnical services, USA) to maintain the temperature. For comparison NPs were also prepared using normal desolvation technique without polysorbate 80 and incubation prior to the addition of ethanol.

2.4. Factors affecting quality of nanoparticles

A variety of product and process parameters were identified using the Ishikawa's diagram to delineate potential cause and effect relationship on the critical quality attributes (CQAs) of Iro-HSA-NPs (Fig.S1). CQAs influencing the product performance were selected as particle size,

polydispersity index (PDI), drug loading (DL) and entrapment efficiency (EE). Further risk estimation matrix (REM) (Table S 1) helped with qualitative analysis of low, medium and high risk related toproduct parameters and process parameters influencing the CQAs of Iro-HSA-NPs. The parameters at high risk have an increased probability of affecting the CQAs and were further identified and analyzed.

Some of the factors such as the choice of desolvating agent,its addition rate, stirring speed were determined according to the literature and confirmed with initial screening (Maghsoudi et al., 2008). Incubation time and concentration of polysorbate 80 were defined and optimized prior to desolvation. The other factors such as ethanol concentration and homogenization pressure were also optimized. Iro:HSA ratio and crosslinking temperature considered as the most critical factors affecting entrapment efficiency and drug loading remained undefined. These two factors vary with the type and amount of drug, so required cooperative optimization to get maximum entrapment and loading of Iro.

2.5. Design of experiment by 3^2 factorial design

The two most influential factors Iro:HSA ratio and the crosslinking temperature were optimised using 3^2 factorial design (Design Expert® 10 software) keeping the other factors constant.HSA concentration was varied from 10 to 30 mg/mL with Iro concentration at 1mg/mL giving Iro: HSA ratio (X_1) of 1:10, 1:20 and 1:30. Whereas, homogenization crosslinking temperatures (X_2) selected were 50, 55 and 60^0C. These two input factors were coded as X_1 and X_2 with their levels coded -1, 0 and +1. Particle size (Y_1), PDI (Y_2), % EE (Y_3), and %DL (Y_4) were considered as the response variables.

2.6. Freeze drying of Iro-HSA-NPs

Iro-HSA-NPs were freeze dried in Epsilon 2- 4 LSC freeze dryer (Martin Christ, Germany) with 30 hour cycle including primary drying at the shelf temperature of -50^0C for 5 hours followed by an increase in temperature to -25^0C at the pressure of 0.10 mbar for 20 hours. Secondary drying was carried out by increasing the temperature up to 25^0C at 0.01 mbar for next 5 hours (Anhorn et al., 2008). Trehalose and mannitol were investigated as cryoprotectant to inhibit the particle growth during lyophilization.

2.7. Characterization of Iro-HSA-NPs

2.7.1 Particle size and Polydispersity Index (PDI)

For the determination of particle size and PDI, samples were diluted with double distilled water in polystyrene cuvettes and measured at a temperature of 25°C and a scattering angle of 90° by dynamic light scattering (DLS) using Beckman coulter N5 Particle size analyzer (Beckman, USA). PDI was also measured to characterize the size distribution. The results are reported as the average of three values.

2.7.2 Zeta potentialMeasurement

Zeta Potential of the particles was determined using Zetasizer (Malvern instrument Ltd, UK) at 25°C after making suitable dilution with de-ionized double distilled water.

2.7.3 Entrapment Efficiency (% EE)

To assess the drug entrapment in Iro-HSA-NPs, 1 mL of sample was centrifuged at 60,000 rpm for 120 minutes using Beckman coulter optima MAX-XP ultracentrifuge (Beckman, USA). Supernatant was analyzed for the Iro and entrapment efficiency was calculated using following equation:

$$\%\boldsymbol{EE} = \frac{(Total\ amount\ of\ Iro\ added - Amount\ of\ Iro\ in\ Supernatant)\ X\ 100}{Total\ Iro\ added} \quad \ldots 2$$

2.7.4 Drug loading (%DL)

Accurately weighed amount of the NPs were added to 1 mL of phosphate buffer saline (pH 7.4). The particles in the solution were degraded by adding trypsin (0.1 mg/mg of NPs) (Dubey et al., 2015). The mixture was stirred overnight, centrifuged and the supernatant was analyzed for drug content. Drug loading was calculated by the following formula:

$$\%\boldsymbol{DL} = \frac{Amount\ of\ Iro\ in\ NPs\ \ X\ 100}{Weight\ of\ NPs} \quad \ldots\ldots\ldots 3$$

2.7.5 Field Emission Gun Surface Electron Microscopy (FEG-SEM)

Surface morphology of both lyophilized Iro-HSA-NPs and Iro-HSA-NPs after reconstitution of lyophilized powder was studied. Samples were prepared by overnight drying on aluminum foil and were transferred to the copper grid and examined under FEG-SEM (JSM-7600F, JEOL, USA) using accelerating voltage of 5kv and magnification up to 40,000X.

2.7.6 Differential Scanning Calorimetry (DSC)

DSC of Iro, HSA and lyophilized Iro-HSA-NPs were performed on a Mettler DSC 823 (Mettler Toledo, Switzerland). The powdered samples were weighed, put into an aluminum pan, and sealed carefully. During measurement, the sample and reference cell were purged with nitrogen gas. The samples were placed in the sample cell and were heated up to 300^0C by increasing the temperature at a rate of 10^0C/minute and thermograms were recorded.

2.7.7 Fourier Transform Infrared (FTIR) Spectroscopy

Infrared spectra were recorded with FTIR spectrometer to study the conformational changes in NPs. FTIR is a prevailing means of identifying types of chemical bonds in a molecule by producing an infrared absorption spectrum. Samples were prepared by KBr pellet method. The sample (0.5 to 1.0 mg) was thoroughly mixed with approximately 100 mg of dry KBr powder. Spectra were scanned from 4000-400 cm^{-1}.

2.7.8 Fluorescence Spectroscopy

The fluorescence spectra of blank HSA NPs and Iro-HSA-NPs were measured after excitation at 280 nm, scanned at an emission wavelength range between 290–400nm at room temperature using Perkin Elmer LS-55 fluorescence spectrometer, USA.

2.7.9 *In vitro* drug release study

To study the release of Iro from Iro-HSA-NP, NPs equivalent to 1mg of Iro were enclosed within dialysis bags (dialyzing membrane-150, molecular weight cut off 12000-14000 Dalton). The dialyzing membrane was soaked for 30 minutes in water prior to use. The dialysis bag was kept in 1000 mL of phosphate buffer saline pH 7.4 or phosphate buffer pH 5 and maintained at 37°C ± 1°Cup to 24 hours with continuous stirring at 500 rpm (Nastase et al., 2014). After fixed time intervals, 2 mL of sample volume were withdrawn and replenished with the fresh buffer to maintain the sink condition. The amount of Iro released in dissolution media was quantified by HPLC.

2.8 Quantification of Iro by HPLC

HPLC was performed on column BDS Hypersil C 18 (250 × 4.6 mm internal diameter, pore size 5 μm; Thermo scientific, USA) with the column temperature of 40^0C using Agilent 1200 HPLC (Agilent Technologies, USA). The mobile phase used was water: acetonitrile (60:40), pH adjusted to 3 with orthophosphoric acid at the fixed flow rate of 0.8ml/min. Iro was detected at 225 nm by PDA detector (Poujol et al., 2003). The amount of Iro in the samples was quantified using calibration curve plotted with known Iro concentrations.

2.9 Short term and long term stability studies

Short-term stability of fresh Iro-HSA-NP dispersions was determined by storing them at 4^0 and 25^0C respectively. Samples were withdrawn after 1, 24, 48, 72 and 96 hours and were analyzed for particle size, PDI and zeta potential. For long-term stability studies, lyophilized Iro-HSA-NPs were stored and packed in sealed glass vials at 4^0C. The samples were withdrawn at 1, 3, 6, 12 and 24 months and were evaluated for any significant changes in the particle size, PDI, zeta potential and entrapment efficiency.

2.10 Statistical analysis

The relationships between responses and variables of all models were derived by DX-10 (Design Expert® 10). The suitability of quadratic models was confirmed by values of $R^2$and one-way analysis of variance (ANOVA). All other experiments were performed in triplicates and data was analyzed by one-way ANOVA with post Bonferroni's test. Differences with p-value<0.05 (*) were considered significant.

3 Result and discussion

3.1 Fluorescence Quenching

HSA shows a strong fluorescence emission with a peak at 340 nm on excitation at 280 nm due to its single tryptophan residue (Trp-214) (Trynda-Lemiesz, 2004). The fluorescence of protein is quenched by the addition of drug which binds to the tryptophan residues (Reichenwallner and Hinderberger, 2013). On addition of different concentrations of Iro to a fixed concentration of HSA solution, proportional decrease in the fluorescence intensity of HSA was observed indicating interaction between HSA and Iro was concentration dependent (Supplementary Fig.S2 a). A blue shift of maximum emission wavelength revealed an increase of hydrophobic amino acid residues formed by the interaction between Iro and HSA (Chen et al., 2016). The micro environmental polarity around the tryptophan residues converted from hydrohilicity to hydrophobicity, folding the peptide chain to form new conformation (Mahesha et al., 2006). Furthermore, the appearance of an isosbestic point in the fluorescence spectra clearly indicated that there was a simple equilibrium between the free HSA and bound one (Sun et al., 2012b). The plot of F0/F versus [Q] showed a linear curve and the slope corresponds to the Ksv value (Supplementary Fig. S2b). The Stern-Volmer plots were linear over the whole concentration range studied and yielded typical Ksv-value of 0.002 X 10^3 $mL.\mu g^{-1}$. Binding constant calculated by plotting log [F0 − F /F] versus log [Q] (Supplementary Fig. S2c) was found to be 3.14 mM^{-1}. Both the Ksv and K revealed that the interaction of Iro with HSA was weak; much lower than other drugs e.g. lapatinib, 5-fluorouracil and captopril (Gao et al., 2011; Kabir et al., 2016; Sun

et al., 2012a). Verily, this also is in consonance with an earlier study, which has reported other proteins to have interacted more with Iro than HSA in a magnetic nanoparticle system (Tamyurek et al., 2015).

The quenching experiments carried out by the addition of Iro and polysorbate 80 separately or together to HSA solution showed quenching of the HSA fluorescence (Fig. 1). Quenching in the fluorescence indicated modification of the microenvironment and conformational changes in HSA molecules due to interaction with the added molecules (Zhang et al., 2008). Among these spectrums, Iro was found to have very low quenching and weak interaction. The results are supported by our earlier experiment elucidating the poor binding constant of Iro-HSA. The quenching exhibited by polysorbate 80 was found to be higher than the Iro and can be described by the strong interaction of polysorbate 80 and HSA to form polysorbate80-HSA complex (Delgado-Magnero et al., 2014). A significantly higher quenching was observed on addition of both Iro and polysorbate 80 to the HSA solution. This could be possibly due to modification of the HSA structure with formation of polysorbate80-HSA complex (Delgado-Magnero et al., 2014), resulting in the increased affinity and improvement in Iro-HSA binding. Change in affinity of drugs to HSA in presence of third compound has been previously reported (Shiri et al., 2017). This approach was further exploited to enhance the encapsulation of Iro in HSA-NPs.

3.2 Risk assessment studies

The CQAs earmarked for Iro-HSA-NPs included particle size, PDI, entrapment efficiency and drug loading. Selection criterion of the CQAs was based upon the prior literature, knowledge and experience on the formulations of HSA NPs. Following the identification of the parameters affecting CQAs; they were ranked according to their criticality in terms of risk. REM was constructed in order to analyze the risk(s) associated with each material attribute and process parameters. The qualitative analysis of each product and process parameter was carried out by ranking them as low, medium and high levels representing the probability of risk and severity of the related effect as presented in Table S1. Based on the REM, the high to medium risk variables were optimized and their effect on CQAs was investigated.

3.3 Preparation of Iro-HSA-NPs

Polysorbate 80 is the most common non-ionic surfactant used in the formulation of various therapeutic products as a solubility enhancer and stabilizing agent (Kerwin, 2008). The addition of polysorbate 80 to HSA can stabilize the protein molecules by directly binding to the hydrophobic surface areas of protein minimizing protein-protein interaction and thus aggregation (Garidel et al., 2009). Secondly, it interacts with the proteins in order to create protein-polysorbate 80 complex and making protein more hydrophilic as compared to native protein (Delgado-Magnero et al., 2014). It has been previously reported that interaction between albumin and polysorbate 80 is not solely driven by the hydrophobic interaction between the surfactant tails and the apolar amino acids of the protein, but there is also a significant contribution from the interactions through the polar heads. The surfactant interacts with the protein predominantly via the polyoxyethylene groups of their polar heads through hydrogen bonds and van der Waals interactions. In addition, polysorbate 80 binds to non-specific surface regions on albumin, self-assembling in clusters over the protein surface as micelles through cooperative hydrophobic interactions with other surfactant molecules in solution, thus increasing the solubility of the surfactant: protein complex (Zadymova et al., 2006). These properties of polysorbate 80 were exploited to prepare the stable HSA NPs of Iro with enhanced drug entrapment and loading. Fig. 2 shows the schematic representation of development of Iro loaded HSA-NPs. For the preparation of Iro-HSA-NPs, polysorbate 80 was added to HSA in order to form the polysorbate80-HSA complexes. Further prolonged incubation with the Iro allowed drug to entrap in the self-assembled clusters of polysorbate 80 over the protein surface. Therefore, 3% w/v of polysorbate 80 (50 fold molar excess than HSA) was added to ensure the complete polysorbate80-HSA interaction and complex formation followed by sufficient incubation time of 3h (Table S2) for drug molecules to be incorporated within the polysorbate 80 micelles (Zadymova et al., 2006). Moreover, polysorbate 80 is well tolerated as excipient for intravenous injection (lyophilized powder) up to 12% according to FDA guidelines on inactive ingredients. Desolvation with ethanol reduced the solubility of HSA in aqueous phase and resulted into the formation of Iro-HSA-NPs. However, precipitation of drug was observed when attempt was

made to prepare the NPs by desolvation without presence of polysorbate 80 incubation clearly indicating the important role of polysorbate 80 in loading of Iro.

After desolvation, cross-linking by glutaraldehyde is generally used to harden the albumin NPs (Elzoghby et al., 2012). Glutaraldehyde has been reported to reduce the number of amino groups on the surface of HSA NPs and also decrease the stability of the carrier system. In addition glutaraldehyde as chemical cross linker also has various kind of toxicity (Zeiger et al., 2005). In our method we combined thermal crosslinking with high-pressure homogenization, that protects the native HSA, avoids denaturation and results in high entrapment and loading of the drug (Desai and Soon-Shiong, 2004; Desai et al., 1999). Moreover, applying high pressure by passing through high pressure homogenizer reduced the particle size to nanoscale and increased the stability of NPs (Kamiya et al., 2009).

3.3 Factors affecting the quality attributes of Iro-HSA-NPs

3.3.1 Polysorbate 80 concentration

Increase in the concentration of polysorbate 80 (1-3% w/v) led to decrease in mean particle size and PDI of the NPs (Fig. 3a). This was found to be in good agreement with our previous report (Sidhaye et al., 2016). Polysorbate 80 was also found to have profound effect on entrapment efficiency and drug loading (Fig. 3b) with maximum being achieved at 3% w/v polysorbate 80 concentration. Much higher concentration of polysorbate 80 than its critical micelle concentration (CMC) in pure water (15mg/L) was required, as CMC of polysorbate 80 is known to increase in the presence of albumins because of protein surfactant interaction (Ruiz-Pe˜naa et al., 2010). Furthermore the self-assembled surfactant clusters of polysorbate 80 over the protein surface enabled higher encapsulation of drug.

3.3.2 Ethanol concentration

Addition of ethanol to the albumin cause phase separation of albumin due to its diminished water solubility forming NPs (Langer et al., 2003). Ethanol concentration has been reported to play an influential role in determining the particle size of HSA NPs. Larger aggregates were generated

during the initial desolvation at lower concentration of ethanol due to the exposure and interaction of hydrophobic chains in protein molecules resulting into the aggregation (Li et al., 2007). A gradual decrease in the particle size and PDI of Iro-HSA-NPs was observed when concentration of ethanol was increased from 50 to 80% v/v (Fig. 3c) not only making the particles with lower particle size but with more uniform distribution. The plausible reason for the decrease in the particle size was the breakdown of larger aggregates formed during the initial desolvation into smaller particles with uniform size. This is in conformance with previous literature reports describing decrease in particle size of NPs with increase in percentage of ethanol (Ghosh et al., 2016; Teng et al., 2012).

3.3.3 Homogenization cycles and pressure

High-pressure homogenization is industrially feasible and scalable process to fabricate the NPs (Desai et al., 2004). NPs prepared at lower homogenization pressure of 200 bars for 8 cycles resulted in the reduction of mean particle size to 302 nm. Escalating pressure to 400 bars (8 cycles) and further to 600 bars (8 cycles) reduced the mean particle size to 78 nm. However, further increase in the pressure to 800 bars did not cause any reduction in particle size and PDI but lead to aggregation of particles (Table 1). Once maximal disintegration of particles has been achieved, additional energy put into the system cannot be used for further size reduction of NPs. The energy put in can only expedite the velocity of the particles, giving them sufficient kinetic energy to circumvent the stabilization resulting in coalescence and increase in mean size (Shegokar et al., 2011). Therefore in this context, homogenization pressure was optimized to 600 bars with 8 cycles to get the smallest NPs size of 78 nm. Previously Zu et al has produced BSA NPs of size 144 nm after seven optimized cycles at the pressure of 800 bars (Zu et al., 2013).

3.3.4 Iro: HSA Ratio

No apparent change in the particle size of NPs was discerned when Iro: HSA ratio was increased from 1:10-1:30 (Fig. 3d). This is similar to observations by Langer et al (Langer et al., 2003). But at Iro HSA ratio of 1:40, abrupt increase in the particle size was visible. This may plausibly be due to high concentration of protein resulting in viscous solution which caused slower

nucleation rates leading to larger particles (Galisteo-González and Molina-Bolívar, 2014; Joye and McClements, 2013). Consequently, high super saturation also speeds up agglomeration through greater incidence of particle collision eventuating larger NPs (Kakran et al., 2012). Entrapment efficiency and drug loading of Iro evidently increased with increase in HSA concentration with maximum being achieved at 1: 30 ratio (Fig. 3e). Higher amounts of HSA effected higher desolvation of the protein substantiating higher encapsulation of drug in the NPs. Further increase in HSA content did not contrive higher entrapment efficiency with consequential decline in percentage of drug loading (Li et al., 2008).

3.3.5 Crosslinking temperature

The thermal cross-linking mechanism has been shown to represent condensation between carboxylic groups and amino groups of adjacent protein chains (Esposito et al., 1996). It was observed that cross-linking temperature had a positive effect on entrapment efficiency and drug loading in Iro-HSA-NPs (Asghar et al., 2014). The entrapment and loading of Iro in HSA NPs was enhanced with increase in crosslinking temperature from 50^0 to 60^0 C (Fig. 3f). Maximum entrapment and drug loading was achieved when NPs were cross-linked at 60^0C. However, further increase in the temperature (>60^0C) lead to the formation of gel (Murata et al., 1993). The temperature during the whole homogenization process was maintained at 60^0 C to obtain higher degree of cross-linking and minimize re-dissolution of NPs in water (Chen et al., 1994). This also ensured high encapsulation of drug. The homogenizer temperature was gradually decreased from 60^0 to 30^0 C during removal of Iro-HSA-NPs from homogenizer to avoid aggregation of the NPs due to sudden temperature change.

3.4 Response surface methodology and construction of model Equation

In a 3^2 factorial design Iro: HSA ratio (X_1) and crosslinking temperature (X_2) at 3 levels were considered as two independent input variables while particle size, polydispersity index (PDI), % entrapment efficiency (%EE), % drug loading (%DL), were considered as response variables (Table 2). The data was analyzed by quadratic model in Design Expert software 10 and results of analysis of variance (ANOVA) are listed in Table 3.

The ANOVA of the regression models demonstrates that the models are highly significant as evident from the high F values (F model for particle size = 31.22, F model for PDI= 5.79, F model for %EE= 335.43 and F model of % DL=31.39). Further, the correlation coefficient (R^2) of 0.9750 (particle size), 0.7433 (PDI), 0.9963 (%EE) and 0.8997 (%DL) presents the goodness of fit of these models. It can be seen from predicted versus actual plot (Fig.S3) that the experimentally measured values are well in line with the predicted values. In all above stated models, the predicted R^2 was found to be in reasonable agreement with the adjusted R^2 i.e. the difference was less than 0.2. Furthermore, adequate precision measures the signal to noise ratio. A ratio greater than 4 is desirable. The ratio of 16.105 (particle size), 7.207 (PDI), 58.95 (%EE) and 14.79 (%DL) indicates an adequate signal and models can be used to navigate the design space. In ANOVA, the p value < 0.05 indicates the significance of model terms. With consideration of p values, the significant terms in particle size were crosslinking temperature (X_2), interaction of Iro: HSA ratio and crosslinking temperature (X_1X_2), with quadratic effect of both factors (X_1^2, X_2^2). However, Iro: HSA ratio (X_1) in the described range did not affect the particle size. For PDI, according to p values, crosslinking temperature (X_2) and quadratic effect of Iro: HSA ratio (X_1^2) were the significant model terms, whereas, no effect of Iro: HSA ratio (X_1) and interaction of both factors (X_1X_2) were observed on PDI. While, the significant factors affecting entrapment efficiency were both Iro: HSA ratio (X1) and crosslinking temperature (X2). Though, no significant interaction and quadratic effects of these two factors were observed. Similarly, the most significant factors affecting drug loading was Iro: HSA ratio. But, there were no effect of crosslinking temperature, interaction and quadratic effects observed. The polynomial equations for the estimation of particle size, PDI, entrapment efficiency and drug loading are as follow:

$$\text{Particle Size} = +71.55 + 0.09X_1 + 1.33X_2 - 2.28X_1X_2 + 3.22X_1^2 + 6.66X_2^2 \ldots\ldots. (4)$$

$$\text{PDI} = +0.19 + 0.045X_1 + 0.071X_2 - 0.031 + 0.15X_1^2 - 0.065X_2^2 \ldots\ldots.. (5)$$

$$\%\ \text{EE} = +60.27 + 9.96X_1 + 7.43X_2 - 0.86X_1X_2 + 1.37X_1^2 + 0.56X_2^2 \ldots\ldots\ldots\ldots(6)$$

$$\% DL = +5.78 + 2.79X_1 + 0.87X_2 + 0.009X_1X_2 - 0.36X_1^2 + 0.95X_2^2 \quad \ldots\ldots\ldots\ldots (7)$$

The visual representation of the effect of factors on four CQAs in the form of 3 D response surface plots is given in Fig. 4. As seen from surface response plot (Fig. 4a), crosslinking temperature has positive effect on particle size. Particle size was found to increase with increase in crosslinking temperature whereas increase in Iro: HSA ratio did not show any significant rise in particle size. Similar effect was observed on PDI (Fig. 4b). PDI increased with increase in crosslinking temperature but was not affected by change in Iro: HSA ratio. It was observed that percent EE was greatly affected by change in both Iro: HSA ratio and crosslinking temperature and maximum %EE was achieved at their highest levels (Fig 4c). Increase in Iro: HSA ratio significantly increased the %DL, where as crosslinking temperature did not have any effect (Fig. 4d).

To understand the tunability of Iro-HSA-NPs, design space was established by overlaying the contour plots for all four-response variables. As shown in Fig. 5a the design space (yellow region) observed was quite broad in the overlay plot for tailored Iro-HSA-NPs (particle size <80nm, PDI <0.4, %EE >70 and %DL >7). To understand the effect of individual response on design space, one response was changed at a time, while other three responses were kept constant. Design space varied according to the tailored responses, which in turn were dependent upon the input factors. If the particle size of NPs was tailored to be below 75nm instead of 80nm, the design space got significantly narrower (Fig. 5b). Tailoring of PDI from 0.4 to <0.3 (Fig 5c) entrapment efficiency >70 to >75% (Fig. 5d) also reduced the design space. However, altering % DL up to 8% did not show much effect on the design space (Fig. 5e). A final overlay plot was constructed to obtain the bespoke Iro-HSA-NPs (particle size <80nm, PDI <0.4, %EE >75% and %DL >9) (Fig. 5f), to meet our target profile of developing the NPs with low particle size and PDI with high drug entrapment and loading.

3.5 Freeze Drying of Iro-HSA-NPs

Lyophilisation is one of the most employed techniques to generate NPs with improved stability (Abdelwahed et al., 2006). Freezing generally creates many destabilizing stresses for NPs.

Generation of ice crystals can mechanically damage NPs apart from augmented interaction due to increased nanoparticle concentration entailing aggregation or fusion (Dadparvar et al., 2014). After lyophilisation, Iro-HSA-NPs were reconstituted with water and were observed for any change in appearance and growth in the particle size (Table 4). Trehalose at 4% w/v concentration was found to be acceptable as cryoprotectant as it resulted in free flowing stable product which could be easily reconstituted to yield a translucent dispersion. The reconstituted dispersion did not show any significant change in particle size or PDI from the one prior to freeze-drying (Table 4). Trehalose is known to impart satisfactory protection from lyophilization of HSA protein, providing stability in the solid state (Han et al., 2007). Trehalose also preserves the HSA NPs during freeze-drying as it forms amorphous glass, which interacts with amorphous protein in the freeze-dried cake (Chang et al., 2005). Additionally, physical isolation of adjacent NPs because of presence of glassy cryoprotectant, reduce the freeze-concentration stress on NPs (Niu and Panyam, 2017). Trehalose containing formulations were superior to mannitol with better size conservation, exhibiting minimal increases in nanoparticle size and PDI following the freeze-drying procedure (Wilson et al., 2012).

3.6 Physiochemical Characterization of NPs

3.6.1 Particle Size, polydispersity index and zeta Potential

Particle size and size distribution are important factor of NPs system that influence the drug release and stability of drug-loaded NPs (Singh and Lillard, 2009). Iro-HSA-NPs were found to have mean particle size of 77.38 nm with PDI of 0.290 (Fig. S4a). HSA a negatively-charged molecule (Langer et al., 2003), when desolvated leads to the formation of intermolecular disulphide bonds that leads to protein aggregation and thus development of NPs with negative charge (Jun et al., 2011). Surface charge also plays an important role in the stability of colloidal particles. Higher charge on NPs leads to the repulsion between particles and thus prevents aggregation (Honary and Zahir, 2013). Iro-HSA-NPs showed zeta potential of -23.50mv (Fig. S4b) which is sufficient to inhibit the particle agglomeration, thus increase the stability (Bhattacharjee, 2016).

3.6.2 Entrapment efficiency and drug loading

High drug loading capacity is prudent for any drug carrier to curtail the amount of solid materials required per mL during injection. The entrapment efficiency and drug loading depends on factors such as the nature of the NPs material, encapsulating drug molecules, medium of nanoparticles fabrication and the type of drug loading method (Merodio et al., 2001). For albumin NPs it further counts on degree of binding between the drug and albumin molecule, leakage of drug and drug diffusion to the dispersed phase (Shen et al., 2008). The entrapment efficiency and drug loading maximized by optimized processes was 79.09% ± 4.37% and 9.62% ± 2.12% respectively.

3.6.3 Field emission gun surface electron microscopy (FESEM)

Surface examination of Iro-HSA-NPs by FESEM confirmed their spherical shape and smooth surface (Fig. 6a). The NPs were found to be present in aggregated form with particle size less than 100nm. The aggregation of NPs observed was due to loss of water content and powdered freeze-dried sample. Surface morphology of NPs was again examined after reconstitution of lyophilized NPs with water for injection, which showed both individual round and aggregated NPs with particle size within 100nm (Fig. 6b). These images further confirmed redispersibility of Iro-HSA-NPs on reconstitution, with trehalose maintaining stability during freeze-drying.

3.6.4 Differential scanning calorimeter (DSC)

The DSC thermogram of pure Iro exhibited an endothermic peak at 213°C corresponding to its melting point (Fig. 6c). An endothermic peak of HSA was observed at 100°C, where as Iro-HSA-NPs exhibited no characteristics melting endotherm of drug indicating there was no crystalline drug present in the NPs (Venkateswarlu and Manjunath, 2004). The drug was present in the amorphous phase and was entrapped in NPs (Sun et al., 2015). This is in affirmation with previous literature reports (Dubey et al., 2015; Wei et al., 2014).

3.6.5 Fourier transmission infrared spectroscopy (FTIR)

FTIR spectroscopy is a useful technique for determining conformational and structural dynamics

of proteins. Amide I band arise due to C=O stretching which ranges from1600 to 1700 cm^{-1}.Amide II band is due to the CH stretching and NH bending mode at ≈ 1548cm^{-1}. Amide III band arise due to CN stretching and NH bending at around 1300 cm^{-1}. Amide I band is considered to be more sensitive than amide II for studying the changes in the structural conformations of the HSA (Sekar et al., 2015). Fig.6d shows the FTIR spectra of HSA, Iro and Iro-HSA-NPs respectively. FTIR spectra of HSA showed the amide A peak at 3464 cm^{-1}which got shifted to 3306 cm^{-1}in Iro-HSA-NPs. Peak corresponding to CH stretching showed change from 2958 to 2924cm^{-1}. Intensity of peaks corresponding to amide II band and I at 1661 cm^{-1} and 1541cm^{-1}were significantly reduced in HSA NPs. There was an alteration observed in the peaks of amide III band from 1305 $cm^{-1}$to 1298 cm^{-1}. The modifications observed inIro-HSA-NPs peaks recommend conformational changes in HSA molecule due to adsorption and entrapment of drug and formation of NPs. This is in good agreement with an earlier report (Rajith and Ravindran, 2014).

3.6.6 Fluorescence Study

Upon excitation at 280nm, quenching in the fluorescence emission of Iro loaded HSA NPs was observed against blank HSA NPs (Fig. 6e). Decrease in the fluorescence intensity with Iro-HSA-NPs could be plausible ascribable to change in microenvironment of tryptophan residue responsible for producing fluorescence, suggesting conformational changes in HSA due to interaction of Iro, polysorbate 80 and HSA in NPs (Gong et al., 2015; Rohiwal et al., 2015).

In vitro drug release

Iro-HSA-NPs showed biphasic drug release, displaying initial burst release (20-25%) of drug in first thirty minutes of dissolution followed by the sustained release up to 24 hours (Fig 6f). This burst release can be credited to the weakly bound drug on the surface of NPs in polysorbate 80 clusters. Later, the entrapped Iro released from the core of the NPs in a sustained manner due to the diffusion of drug across the albumin matrix, would give the opportunity of continual drug effect.

3.7 Short term stability studies

For short-term stability studies Iro-HSA-NPs aqueous dispersions prepared under optimized conditions were kept at 4^0C and 25^0 C for 96 hours. There was no significant change observed in particle size and zeta potential of NPs stored at 4^0C as well 25^0C, though the nanodispersions became more polydisperse as evidenced by higher PDI values (Fig.7). HSA nanodispersions have shown acceptable stability in previous reports (Dreis et al., 2007).

3.8 Long-term stability studies

Lyophilization, or freeze-drying, is widely used in the pharmaceutical industry to boost the long-stability and increase the shelf life of many drug products by removing the total water content from the drug formulation apart from providing convenience of shipping in dry powder form. The long-term stability study revealed no significant increase in the particle size of Iro-HSA-NPs up to 12 months and was within the desired particle size of 100nm. A uniform particle size distribution was maintained as testified by the PDI of NPs. Previous reports demonstrate that HSA NPs can be stabilized for long-term storage after freeze drying when using adequate concentrations of suitable excipients (Anhorn et al., 2008). A significant increase (p value <0.05) in the particle size was observed after 24 months of storage along with increase in value of PDI (Fig. 8a and b). A decreased stability of Iro-HSA-NPs at the end of 24 months storage was further evidenced by lowered value of zeta potential which could ostensibly lead to agglomeration of NPs (Fig. 8c). Particle growth had no effect on entrapped drug as entrapment efficiency remained within acceptable limits even after 24 months (Fig. 8d).

4 Conclusion

In the present study, we have successfully prepared HSA NPs of a slightly soluble drug Iro having average albumin binding affinity by modified desolvation technique. Addition of polysorbate 80 into HSA solution resulted into polysorbate 80-HSA complex with self-assembling clusters of polysorbate 80 over the protein surface in form of micelles that were able to entrap Iro during formation of Iro-HSA-NPs. The optimized process has led to the production of the Iro-HSA-NPs with particle size less than 80 nm. Successful entrapment of drug in NPs

was confirmed by DSC, FTIR and fluorescence spectroscopy. The response surface graph clearly explained the positive effect of two critical factors (Iro: HSA ratio and crosslinking temperature) on entrapment efficiency and drug loading properties of NPs. These factors can be tailored to obtain the bespoke NPS with tunable particle size and drug loading. Lyophilization of Iro-HSA-NPs resulted in good stability till 12-month period. Thus, the prepared NPs of Iro seem promising drug delivery system due to their small particle size, high drug entrapment and drug loading capacity. These drug loaded Iro-HSA-NPs also release drug in controlled manner for prolonged period of time, which would enhance the bioavailability of the drug to target site. Further studies are in progress to establish their pharmacokinetics and pharmacodynamics to harness their therapeutic potential as a drug delivery system.

Acknowledgements

Financial grants received from the University Grant Commission (UGC), New Delhi, India, for research assistance is acknowledged. The author Neetika Taneja is grateful to UGC for providing financial grant to her to carry out the present work as a Research Fellow under BSR fellowship (F.7162/2007(BSR) dated10 June 2012). We also acknowledge IIT Mumbai for carrying out FEG-SEM and FTIR.

Declaration of Interest

Authors declare no conflict(s) interest.

References:

Abdelwahed, W., Degobert, G., Stainmesse, S., Fessi, H., 2006. Freeze-drying of nanoparticles: formulation, process and storage considerations. Advanced drug delivery reviews 58, 1688-1713.

Anand, U., Mukherjee, S., 2013. Binding, unfolding and refolding dynamics of serum albumins. Biochimica et Biophysica Acta (BBA)-General Subjects 1830, 5394-5404.

Anhorn, M.G., Mahler, H.-C., Langer, K., 2008. Freeze drying of human serum albumin (HSA) nanoparticles with different excipients. International Journal of Pharmaceutics 363, 162-169.

Asghar, S., Salmani, J.M.M., Hassan, W., Xie, Y., Meng, F., Su, Z., Sun, M., Xiao, Y., Ping, Q., 2014. A facile approach for crosslinker free nano self assembly of protein for anti-tumor drug delivery: Factors' optimization, characterization and in vitro evaluation. European Journal of Pharmaceutical Sciences 63, 53-62.

Barnhart, J., LEVENE, H., VILLAPANDO, E., MANIQUIS, J., FERNANDEZ, J., RICE, S., Jablonski, E., GJØEN, T., TOLLESHAUG, H., 1990. Characteristics of Albunex Air-Filled Albumin Microspheres for Echocardiography Contrast Enhancement. Investigative Radiology 25, S162-S164.

Bhattacharjee, S., 2016. DLS and zeta potential–What they are and what they are not? Journal of Controlled Release 235, 337-351.

Chang, L.L., Shepherd, D., Sun, J., Ouellette, D., Grant, K.L., Tang, X.C., Pikal, M.J., 2005. Mechanism of protein stabilization by sugars during freeze‐drying and storage: Native structure preservation, specific interaction, and/or immobilization in a glassy matrix? Journal of Pharmaceutical Sciences 94, 1427-1444.

Chen, G., Lin, W., Coombes, A., Davis, S., Illum, L., 1994. Preparation of human serum albumin microspheres by a novel acetone-heat denaturation method. Journal of Microencapsulation 11, 395-407.

Chen, Y.-C., Wang, H.-M., Niu, Q.-X., Ye, D.-Y., Liang, G.-W., 2016. Binding between Saikosaponin C and Human Serum Albumin by Fluorescence Spectroscopy and Molecular Docking. Molecules 21, 153.

Ci, T., Chen, L., Yu, L., Ding, J., 2014. Tumor regression achieved by encapsulating a moderately soluble drug into a polymeric thermogel. Scientific Reports 4.

Combes, O., Barré, J., Duché, J.-C., Vernillet, L., Archimbaud, Y., Marietta, M., Tillement, J.-P., Urien, S., 2000. In Vitro Binding and Partitioning of Irinotecan (CPT-11) and its Metabolite, SN-38, in Human Blood. Invest New Drugs 18, 1-5.

Cortes, J., Saura, C., 2010. Nanoparticle albumin-bound (nab™)-paclitaxel: improving efficacy and tolerability by targeted drug delivery in metastatic breast cancer. European Journal of Cancer Supplements 8, 1-10.

Dadparvar, M., Wagner, S., Wien, S., Worek, F., von Briesen, H., Kreuter, J., 2014. Freeze-drying of HI-6-loaded recombinant human serum albumin nanoparticles for improved storage stability. European Journal of Pharmaceutics and Biopharmaceutics 88, 510-517.

De, M., Rana, S., Akpinar, H., Miranda, O.R., Arvizo, R.R., Bunz, U.H., Rotello, V.M., 2009. Sensing of proteins in human serum using conjugates of nanoparticles and green fluorescent protein. Nature Chemistry 1, 461-465.

Delgado-Magnero, K.H., Valiente, P.A., Ruiz-Peña, M., Pérez-Gramatges, A., Pons, T., 2014. Unraveling the binding mechanism of polyoxyethylene sorbitan esters with bovine serum albumin: A novel theoretical model based on molecular dynamic simulations. Colloids and Surfaces B: Biointerfaces 116, 720-726.

Desai, N., 2007. Nanoparticle albumin bound (nab) technology: targeting tumors through the endothelial gp60 receptor and SPARC. Nanomedicine: Nanotechnology, Biology and Medicine 3, 339.

Desai, N.P., Soon-Shiong, P., 2004. Paclitaxel-containing formulations. US 6753006 B1

Desai, N.P., Tao, C., Yang, A., Louie, L., Yao, Z., Soon-Shiong, P., Magdassi, S., 2004. Protein stabilized pharmacologically active agents, methods for the preparation thereof and methods for the use thereof. U.S. Patent 6749868 B1.

Desai, N.P., Tao, C., Yang, A., Louie, L., Zheng, T., Yao, Z., Soon-Shiong, P., Magdassi, S., 1999. Protein stabilized pharmacologically active agents, methods for the preparation thereof and methods for the use thereof. US 5916596 A.

dos Santos, K.S.C.R., Silva, H.S.R.C., Ferreira, E.I., Bruns, R.E., 2005. 32 Factorial design and response surface analysis optimization of N-carboxybutylchitosan synthesis. Carbohydrate Polymers 59, 37-42.

Douillard, J.Y., Cunningham, D., Roth, A.D., Navarro, M., James, R.D., Karasek, P., Jandik, P., Iveson, T., Carmichael, J., Alakl, M., Gruia, G., Awad, L., Rougier, P., 2000. Irinotecan

combined with fluorouracil compared with fluorouracil alone as first-line treatment for metastatic colorectal cancer: a multicentre randomised trial. The Lancet 355, 1041-1047.

Dreis, S., Rothweiler, F., Michaelis, M., Cinatl, J., Kreuter, J., Langer, K., 2007. Preparation, characterisation and maintenance of drug efficacy of doxorubicin-loaded human serum albumin (HSA) nanoparticles. International Journal of Pharmaceutics 341, 207-214.

Dubey, R.D., Alam, N., Saneja, A., Khare, V., Kumar, A., Vaidh, S., Mahajan, G., Sharma, P.R., Singh, S.K., Mondhe, D.M., 2015. Development and evaluation of folate functionalized albumin nanoparticles for targeted delivery of gemcitabine. International Journal of Pharmaceutics 492, 80-91.

Elzoghby, A.O., Samy, W.M., Elgindy, N.A., 2012. Albumin-based nanoparticles as potential controlled release drug delivery systems. Journal of Controlled Release 157, 168-182.

Esposito, E., Cortesi, R., Nastruzzi, C., 1996. Gelatin microspheres: influence of preparation parameters and thermal treatment on chemico-physical and biopharmaceutical properties. Biomaterials 17, 2009-2020.

Fuchs, C., Mitchell, E.P., Hoff, P.M., 2006. Irinotecan in the treatment of colorectal cancer. Cancer Treatment Reviews 32, 491-503.

Galisteo-González, F., Molina-Bolívar, J., 2014. Systematic study on the preparation of BSA nanoparticles. Colloids and Surfaces B: Biointerfaces 123, 286-292.

Gao, X., Tang, Y., Rong, W., Zhang, X., Zhao, W., Zi, Y., 2011. Analysis of binding interaction between Captopril and human serum albumin. American Journal of Analytical Chemistry 2, 250.

Garidel, P., Hoffmann, C., Blume, A., 2009. A thermodynamic analysis of the binding interaction between polysorbate 20 and 80 with human serum albumins and immunoglobulins: A contribution to understand colloidal protein stabilisation. Biophysical Chemistry 143, 70-78.

Ghosh, P., Roy, A.S., Chaudhury, S., Jana, S.K., Chaudhury, K., Dasgupta, S., 2016. Preparation of albumin based nanoparticles for delivery of fisetin and evaluation of its cytotoxic activity. International Journal of Biological Macromolecules 86, 408-417.

Gong, G., Pan, Q., Wang, K., Wu, R., Sun, Y., Lu, Y., 2015. Curcumin-incorporated albumin nanoparticles and its tumor image. Nanotechnology 26, 045603.

Green, M., Manikhas, G., Orlov, S., Afanasyev, B., Makhson, A., Bhar, P., Hawkins, M., 2006. Abraxane®, a novel Cremophor®-free, albumin-bound particle form of paclitaxel for the treatment of advanced non-small-cell lung cancer. Annals of Oncology 17, 1263-1268.

Guo, M., Rong, W.-T., Hou, J., Wang, D.-F., Lu, Y., Wang, Y., Yu, S.-Q., Xu, Q., 2013. Mechanisms of chitosan-coated poly (lactic-co-glycolic acid) nanoparticles for improving oral absorption of 7-ethyl-10-hydroxycamptothecin. Nanotechnology 24, 245101.

Han, Y., Jin, B.-S., Lee, S.-B., Sohn, Y., Joung, J.-W., Lee, J.-H., 2007. Effects of sugar additives on protein stability of recombinant human serum albumin during lyophilization and storage. Archives of Pharmacal Research 30, 1124.

Hardman, W., Moyer, M., Cameron, I., 1999. Fish oil supplementation enhanced CPT-11 (irinotecan) efficacy against MCF7 breast carcinoma xenografts and ameliorated intestinal side-effects. British Journal of Cancer 81, 440.

Honary, S., Zahir, F., 2013. Effect of zeta potential on the properties of nano-drug delivery systems-a review (Part 2). Tropical Journal of Pharmaceutical Research 12, 265-273.

Joye, I.J., McClements, D.J., 2013. Production of nanoparticles by anti-solvent precipitation for use in food systems. Trends in food science & technology 34, 109-123.

Jun, J.Y., Nguyen, H.H., Chun, H.S., Kang, B.-C., Ko, S., 2011. Preparation of size-controlled bovine serum albumin (BSA) nanoparticles by a modified desolvation method. Food Chemistry 127, 1892-1898.

Kabir, M.Z., Mukarram, A.K., Mohamad, S.B., Alias, Z., Tayyab, S., 2016. Characterization of the binding of an anticancer drug, lapatinib to human serum albumin. Journal of Photochemistry and Photobiology B: Biology 160, 229-239.

Kakran, M., Sahoo, N.G., Li, L., Judeh, Z., 2012. Fabrication of quercetin nanoparticles by anti-solvent precipitation method for enhanced dissolution. Powder Technology 223, 59-64.

Kamali, M., Dinarvand, R., Maleki, H., Arzani, H., Mahdaviani, P., Nekounam, H., Adabi, M., Khosravani, M., 2015. Preparation of imatinib base loaded human serum albumin for application in the treatment of glioblastoma. RSC Advances 5, 62214-62219.

Kamiya, S., Kurita, T., Miyagishima, A., Arakawa, M., 2009. Preparation of griseofulvin nanoparticle suspension by high-pressure homogenization and preservation of the suspension with saccharides and sugar alcohols. Drug Development and Industrial Pharmacy 35, 1022-1028.

Kerwin, B.A., 2008. Polysorbates 20 and 80 used in the formulation of protein biotherapeutics: structure and degradation pathways. Journal of Pharmaceutical Sciences 97, 2924-2935.

Kratz, F., 2008. Albumin as a drug carrier: design of prodrugs, drug conjugates and nanoparticles. Journal of Controlled Release 132, 171-183.

Kumar, P.V., Jain, N.K., 2007. Suppression of agglomeration of ciprofloxacin-loaded human serum albumin nanoparticles. AAPS PharmSciTech 8, E118-E123.

Langer, K., Balthasar, S., Vogel, V., Dinauer, N., von Briesen, H., Schubert, D., 2003. Optimization of the preparation process for human serum albumin (HSA) nanoparticles. International Journal of Pharmaceutics 257, 169-180.

Lee, S.H., Heng, D., Ng, W.K., Chan, H.-K., Tan, R.B., 2011. Nano spray drying: a novel method for preparing protein nanoparticles for protein therapy. International Journal of Pharmaceutics 403, 192-200.

Li, F.-Q., Su, H., Wang, J., Liu, J.-Y., Zhu, Q.-G., Fei, Y.-B., Pan, Y.-H., Hu, J.-H., 2008. Preparation and characterization of sodium ferulate entrapped bovine serum albumin nanoparticles for liver targeting. International Journal of Pharmaceutics 349, 274-282.

Li, X., Li, Y., Hua, Y., Qiu, A., Yang, C., Cui, S., 2007. Effect of concentration, ionic strength and freeze-drying on the heat-induced aggregation of soy proteins. Food Chemistry 104, 1410-1417.

Maghsoudi, A., Shojaosadati, S.A., Farahani, E.V., 2008. 5-Fluorouracil-loaded BSA nanoparticles: formulation optimization and in vitro release study. AAPS Pharmscitech 9, 1092-1096.

MaHam, A., Tang, Z., Wu, H., Wang, J., Lin, Y., 2009. Proteinuorouracil-loaded BSA nanoparticles: formulation optimization and in

Mahesha, H., Singh, S.A., Srinivasan, N., Rao, A., 2006. A spectroscopic study of the interaction of isoflavones with human serum albumin. Febs Journal 273, 451-467.

Merodio, M., Arnedo, A., Renedo, M.J., Irache, J.M., 2001. Ganciclovir-loaded albumin nanoparticles: characterization and in vitro release properties. European Journal of Pharmaceutical Sciences 12, 251-259.

Murata, M., Tani, F., Higasa, T., Kitabatake, N., Doi, E., 1993. Heat-induced transparent gel formation of bovine serum albumin. Bioscience, Biotechnology, and Biochemistry 57, 43-46.

Nastase, S., Bajenaru, L., Berger, D., Matei, C., Moisescu, M.G., Constantin, D., Savopol, T., 2014. Mesostructured silica matrix for irinotecan delivery systems. Central European Journal of Chemistry 12, 813-820.

Niu, L., Panyam, J., 2017. Freeze concentration-induced PLGA and polystyrene nanoparticle aggregation: Imaging and rational design of lyoprotection. Journal of Controlled Release 248, 125-132.

Passero Jr, F.C., Grapsa, D., Syrigos, K.N., Saif, M.W., 2016. The safety and efficacy of Onivyde (irinotecan liposome injection) for the treatment of metastatic pancreatic cancer following gemcitabine-based therapy. Expert review of anticancer therapy 16, 697-703.

Poujol, S., Pinguet, F., Malosse, F., Astre, C., Ychou, M., Culine, S., Bressolle, F., 2003. Sensitive HPLC-fluorescence method for irinotecan and four major metabolites in human plasma and saliva: application to pharmacokinetic studies. Clinical Chemistry 49, 1900-1908.

Rajith, B., Ravindran, A., 2014. BSA nanoparticle loaded atorvastatin calcium-a new facet for an old drug. PloS One 9, e86317.

Reichenwallner, J., Hinderberger, D., 2013. Using bound fatty acids to disclose the functional structure of serum albumin. Biochimica et Biophysica Acta (BBA)-General Subjects 1830, 5382-5393.

Rohiwal, S., Satvekar, R., Tiwari, A., Raut, A., Kumbhar, S., Pawar, S., 2015. Investigating the influence of effective parameters on molecular characteristics of bovine serum albumin nanoparticles. Applied Surface Science 334, 157-164.

Samant, M., Banerjee, S.S., Taneja, N., Zope, K., Ghogale, P., Khandare, J.J., 2014. Biophysical interactions of polyamidoamine dendrimer coordinated Fe3O4 nanoparticles with insulin. Journal of Biomedical Nanotechnology 10, 1286-1293.

Sekar, G., Sugumar, S., Mukherjee, A., Chandrasekaran, N., 2015. Multiple spectroscopic studies of the structural conformational changes of human serum albumin—Essential oil based nanoemulsions conjugates. Journal of Luminescence 161, 187-197.

Shegokar, R., Singh, K., Müller, R., 2011. Production & stability of stavudine solid lipid nanoparticles—From lab to industrial scale. International Journal of Pharmaceutics 416, 461-470.

Shen, Z.-Y., Ma, G.-H., Dobashi, T., Maki, Y., Su, Z.-G., 2008. Preparation and characterization of thermo-responsive albumin nanospheres. International journal of pharmaceutics 346, 133-142.

Sheng, Z., Hu, D., Zheng, M., Zhao, P., Liu, H., Gao, D., Gong, P., Gao, G., Zhang, P., Ma, Y., 2014. Smart human serum albumin-indocyanine green nanoparticles generated by programmed assembly for dual-modal imaging-guided cancer synergistic phototherapy. ACS Nano 8, 12310-12322.

Shiri, F., Shahraki, S., Shahriyar, A., Majd, M.H., 2017. Exploring isoxsuprine hydrochloride binding with human serum albumin in the presence of folic acid and ascorbic acid using multispectroscopic and molecular modeling methods. Journal of Photochemistry and Photobiology B: Biology.

Sidhaye, A.A., Bhuran, K.C., Zambare, S., Abubaker, M., Nirmalan, N., Singh, K.K., 2016. Bio-inspired artemether-loaded human serum albumin nanoparticles for effective control of malaria-infected erythrocytes. Nanomedicine 11, 2809-2828.

Singh, R., Lillard, J.W., 2009. Nanoparticle-based targeted drug delivery. Experimental and Molecular Pathology 86, 215-223.

Sleep, D., 2015. Albumin and its application in drug delivery. Expert opinion on drug delivery 12, 793-812.

Sobrero, A.F., Maurel, J., Fehrenbacher, L., Scheithauer, W., Abubakr, Y.A., Lutz, M.P., Vega-Villegas, M.E., Eng, C., Steinhauer, E.U., Prausova, J., 2008. EPIC: phase III trial of cetuximab plus irinotecan after fluoropyrimidine and oxaliplatin failure in patients with metastatic colorectal cancer. Journal of clinical oncology 26, 2311-2319.

Sun, H., Wu, Y., He, P., Zuo, Y., Lv, Y., 2012a. Characterization of interaction between antitumor drug 5-fluorouracil and human serum albumin by affinity capillary electrophoresis. Asian Journal of Pharmaceutical Sciences 7, 75-79.

Sun, S.-B., Liu, P., Shao, F.-M., Miao, Q.-L., 2015. Formulation and evaluation of PLGA nanoparticles loaded capecitabine for prostate cancer. International Journal of Clinical and Experimental Medicine 8, 19670.

Sun, Y., Ji, Z., Liang, X., Li, G., Yang, S., Wei, S., Zhao, Y., Hu, X., Fan, J., 2012b. Studies on the binding of rhaponticin with human serum albumin by molecular spectroscopy, modeling and equilibrium dialysis. Spectrochimica Acta Part A: Molecular and Biomolecular Spectroscopy 87, 171-178.

Tamyurek, E., Maltas, E., Bas, S.Z., Ozmen, M., Yildiz, S., 2015. Magnetic nanoparticles–serum proteins bioconjugates for binding of irinotecan. International Journal of Biological Macromolecules 73, 76-83.

Teng, Z., Luo, Y., Wang, Q., 2012. Nanoparticles synthesized from soy protein: preparation, characterization, and application for nutraceutical encapsulation. Journal of Agricultural and Food Chemistry 60, 2712-2720.

Trynda-Lemiesz, L., 2004. Paclitaxel–HSA interaction. Binding sites on HSA molecule. Bioorganic & medicinal chemistry 12, 3269-3275.

Valencia, P.M., Pridgen, E.M., Perea, B., Gadde, S., Sweeney, C., Kantoff, P.W., Bander, N.H., Lippard, S.J., Langer, R., Karnik, R., 2013. Synergistic cytotoxicity of irinotecan and cisplatin in dual-drug targeted polymeric nanoparticles. Nanomedicine 8, 687-698.

Venkateswarlu, V., Manjunath, K., 2004. Preparation, characterization and in vitro release kinetics of clozapine solid lipid nanoparticles. Journal of Controlled Release 95, 627-638.

Waterhouse, D.N., Sutherland, B.W., Dos Santos, N., Masin, D., Osooly, M., Strutt, D., Ostlund, C., Anantha, M., Harasym, N., Manisali, I., 2014. Irinophore C™, a lipid nanoparticle formulation of irinotecan, abrogates the gastrointestinal effects of irinotecan in a rat model of clinical toxicities. Invest New Drugs 32, 1071-1082.

Weber, C., Coester, C., Kreuter, J., Langer, K., 2000. Desolvation process and surface characterisation of protein nanoparticles. International Journal of Pharmaceutics 194, 91-102.

Wei, Y., Li, L., Xi, Y., Qian, S., Gao, Y., Zhang, J., 2014. Sustained release and enhanced bioavailability of injectable scutellarin-loaded bovine serum albumin nanoparticles. International Journal of Pharmaceutics 476, 142-148.

Wilson, B., Ambika, T., Patel, R.D.K., Jenita, J.L., Priyadarshini, S., 2012. Nanoparticles based on albumin: Preparation, characterization and the use for 5-flurouracil delivery. International Journal of Biological Macromolecules 51, 874-878.

Yadav, A.A., Vadali, S., 2008. Preparation of water-soluble albumin loaded paclitaxil nanoparticles using emulsion-solvent evaporation technique. Current Bioactive Compounds 4, 51-55.

Yu, S., Yao, P., Jiang, M., Zhang, G., 2006. Nanogels prepared by selfaded paclitaxil nanoparticles using emulsion-solvent evaporation technique.

Zadymova, N., Yampol'skaya, G., Filatova, L.Y., 2006. Interaction of bovine serum albumin with nonionic surfactant Tween 80 in aqueous solutions: Complexation and association. Colloid Journal 68, 162-172.

Zeiger, E., Gollapudi, B., Spencer, P., 2005. Genetic toxicity and carcinogenicity studies of glutaraldehyde—a review. Mutation Research/Reviews in Mutation Research 589, 136-151.

Zhang, G., Que, Q., Pan, J., Guo, J., 2008. Study of the interaction between icariin and human serum albumin by fluorescence spectroscopy. Journal of Molecular Structure 881, 132-138.

Zhu, K., Ye, T., Liu, J., Peng, Z., Xu, S., Lei, J., Deng, H., Li, B., 2013. Nanogels fabricated by lysozyme and sodium carboxymethyl cellulose for 5-fluorouracil controlled release. International Journal of Pharmaceutics 441, 721-727.

Zu, Y., Meng, L., Zhao, X., Ge, Y., Yu, X., Zhang, Y., Deng, Y., 2013. Preparation of 10-hydroxycamptothecin-loaded glycyrrhizic acid-conjugated bovine serum albumin nanoparticles for hepatocellular carcinoma-targeted drug delivery. International Journal of Nanomedicine 8, 1207.

Figures:.

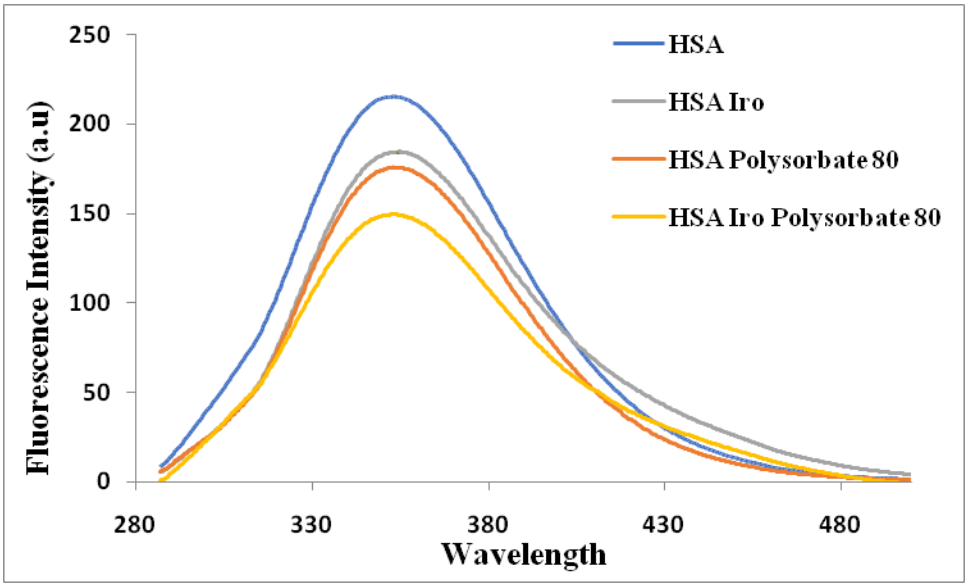

Fig. 1 Overlay of fluorescence spectra of free HSA and HSA in presence of irinotecan (Iro), Polysorbate 80 and Iro Polysorbate 80 combination at λex = 280 nm.

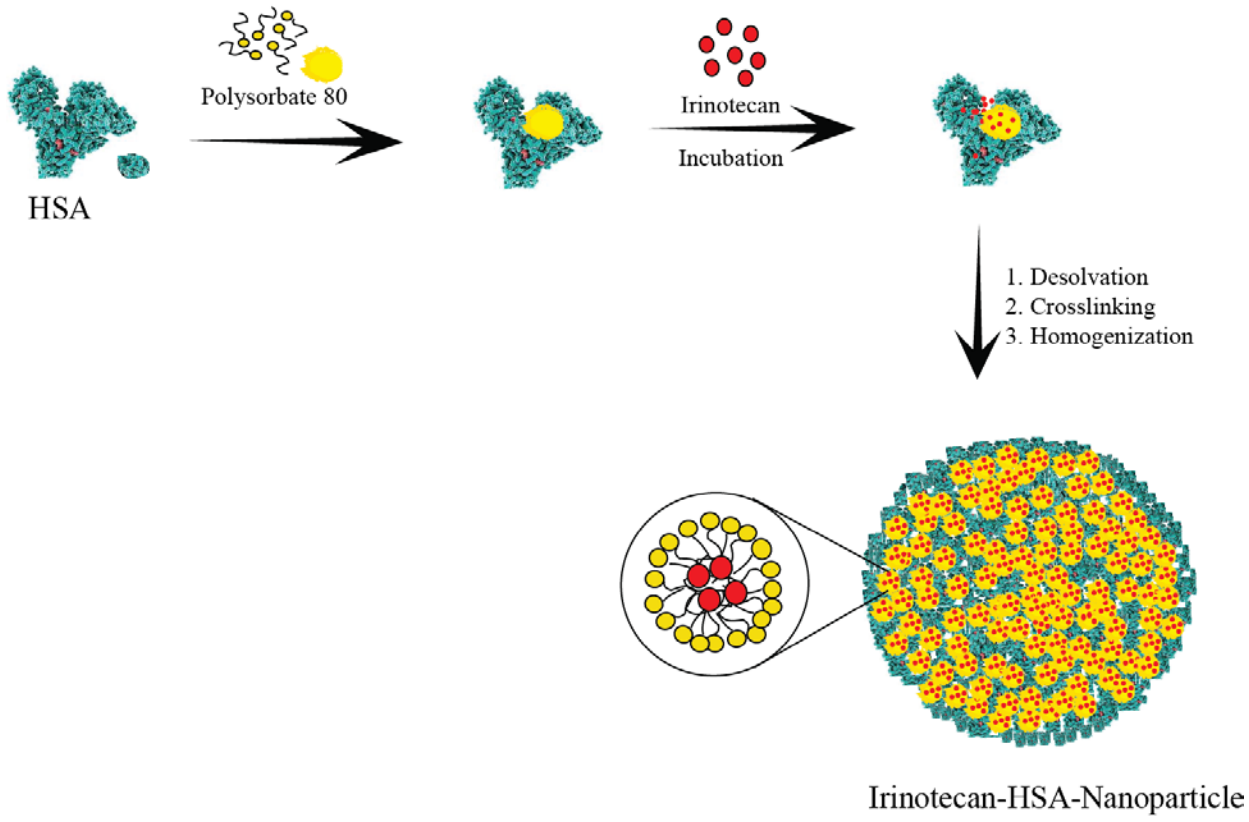

Fig. 2 Schematic diagram for the preparation of Iro-HSA-NPs.

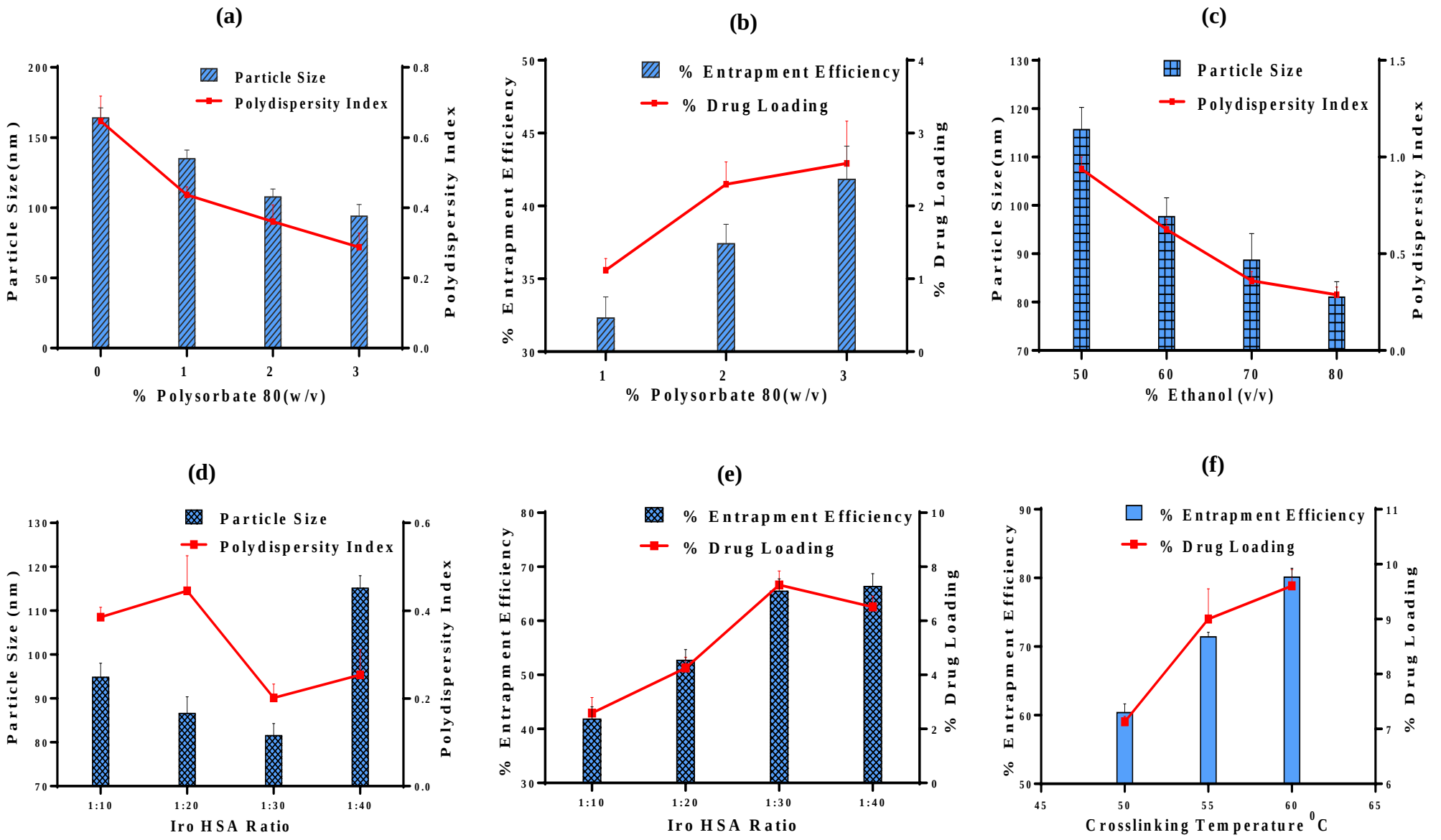

Fig. 3 Effect of polysorbate 80 concentration on (a) particle size and polydispersity index of Iro-HSA-NPs (b) % entrapment efficiency and % drug loading of Iro-HSA-NPs; Effect of (c) Ethanol concentration and (d) Iro: HSA ratioon particle size and polydispersity index of Iro-HSA-NPs; Influence of (e) Iro: HSA ratio and (f) Crosslinking temperatureon % entrapment efficiency and % drug loading of Iro-HSA-NPs.

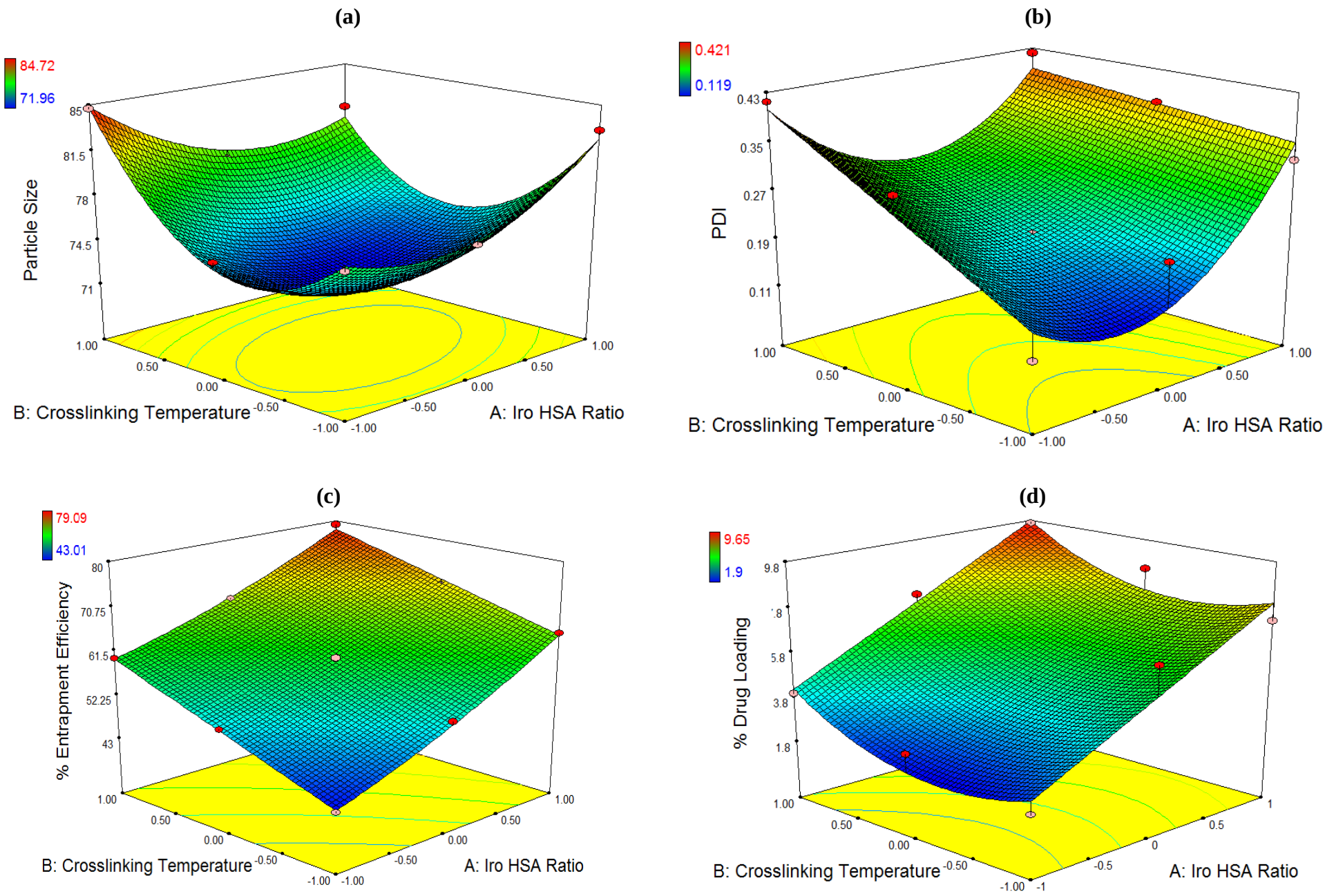

Fig. 4 Response surface plot for the effect of Iro:HSA ratio and crosslinking temperature on (a) particle size (b) polydispersity index (c) % entrapment efficiency and (d) % drug loading of Iro-HSA-NPs.

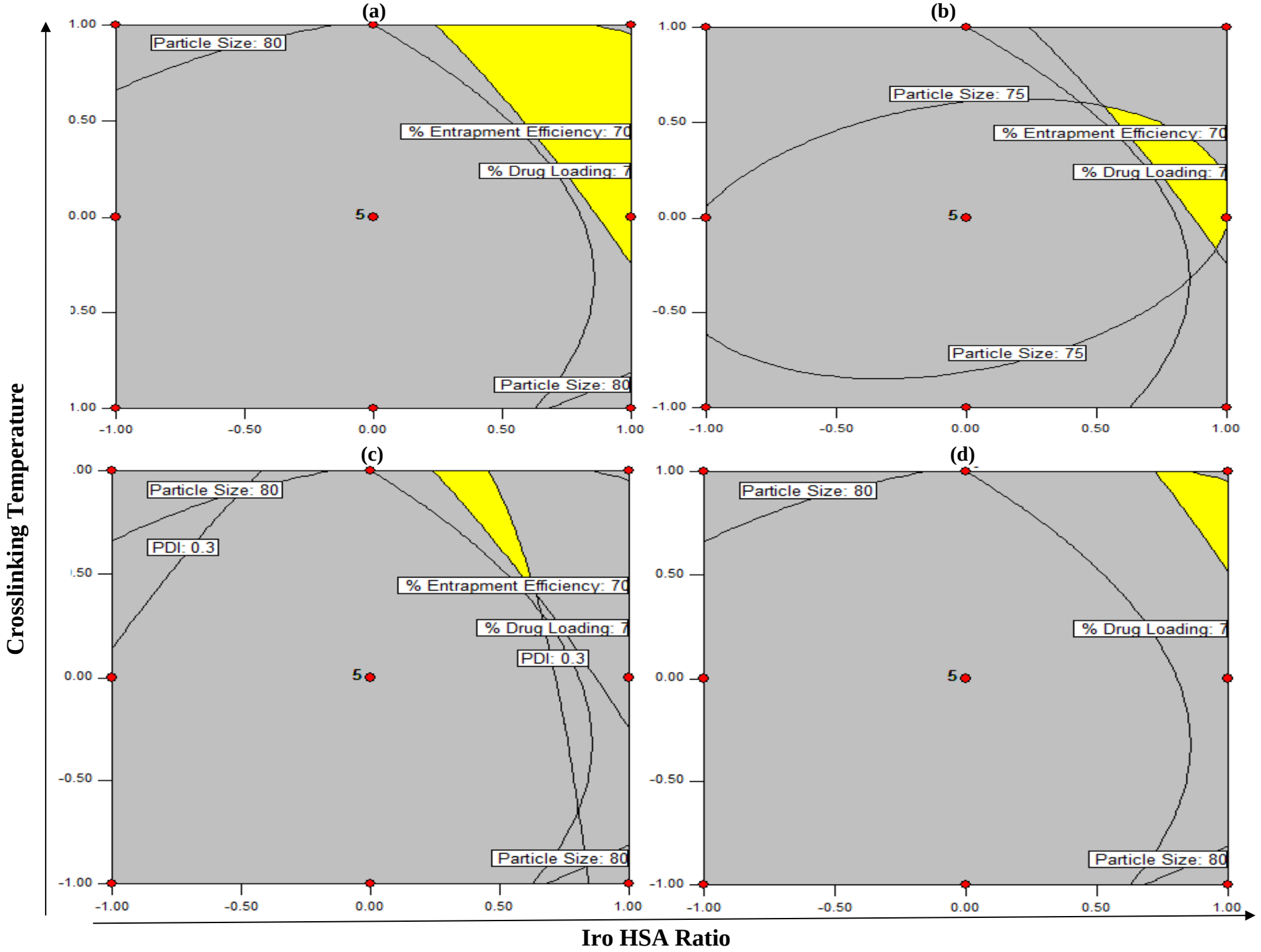
(a)
Particle Size: 80
% Entrapment Efficiency: 70
% Drug Loading: 7
Particle Size: 80
(b)
Particle Size: 75
% Entrapment Efficiency: 70
% Drug Loading: 7
Particle Size: 75
(c)
Particle Size: 80
PDI: 0.3
% Entrapment Efficiency: 70
% Drug Loading: 7
PDI: 0.3
Particle Size: 80
(d)
Particle Size: 80
% Drug Loading: 7
Particle Size: 80
Crosslinking Temperature
Iro HSA Ratio

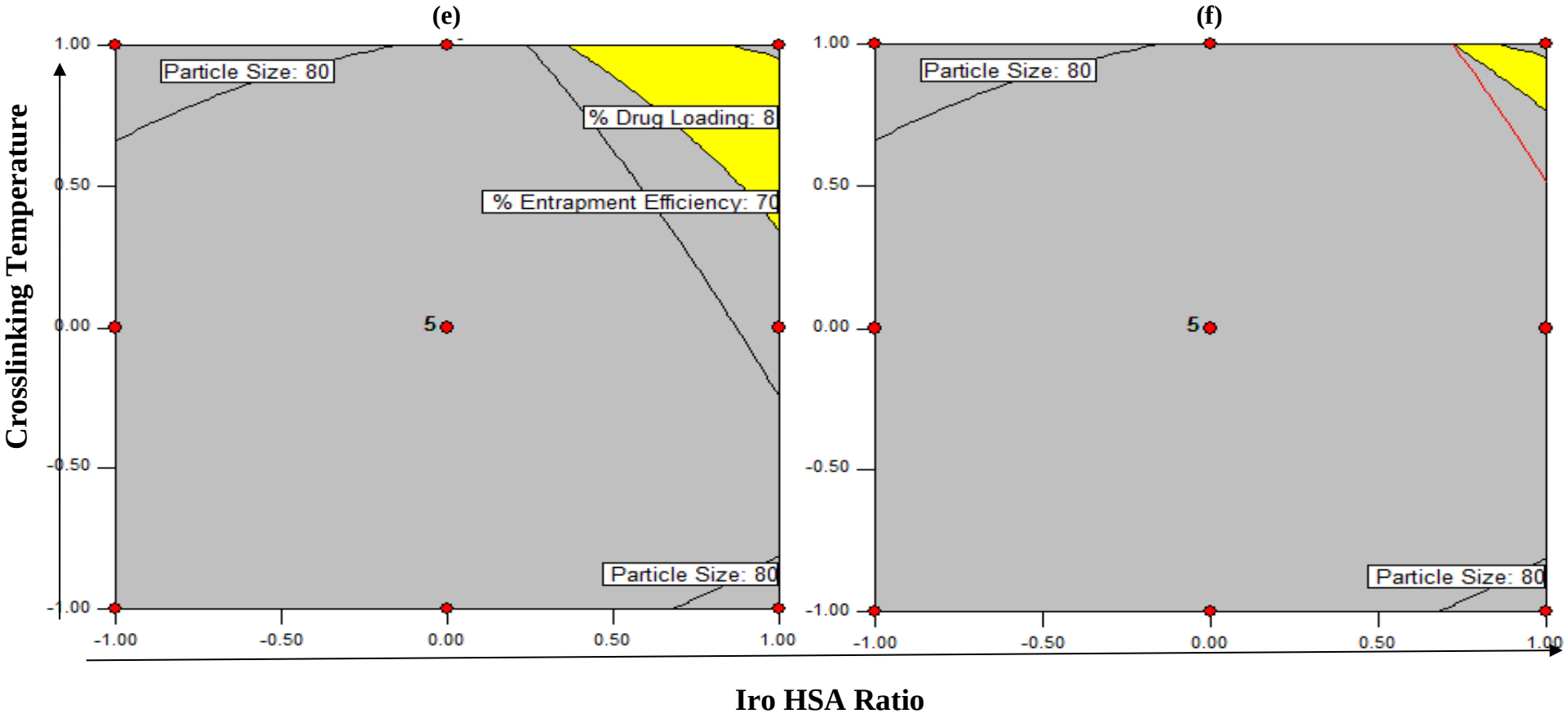

Fig. 5 Overlay counter plot of responses for design space for Iro-HSA-NPs (a) Particle size < 80nm, polydispersity index <0.4, entrapment efficiency >70% and drug loading > 7% (b) Particle size <75nm, polydispersity index <0.4, entrapment efficiency >70% and drug loading >7% (c) Particle size <80nm, polydispersity index <0.3, entrapment efficiency >70% and drug loading >7% (d) Particle size <80nm, polydispersity index <0.4, entrapment efficiency >75% and drug loading >7% (e) Particle size <80nm, polydispersity index<0.4, entrapment efficiency >70% and drug loading >8% (f) Particle size <80nm, polydispersity index <0.4, entrapment efficiency >75% and drug loading >9%.

(a)

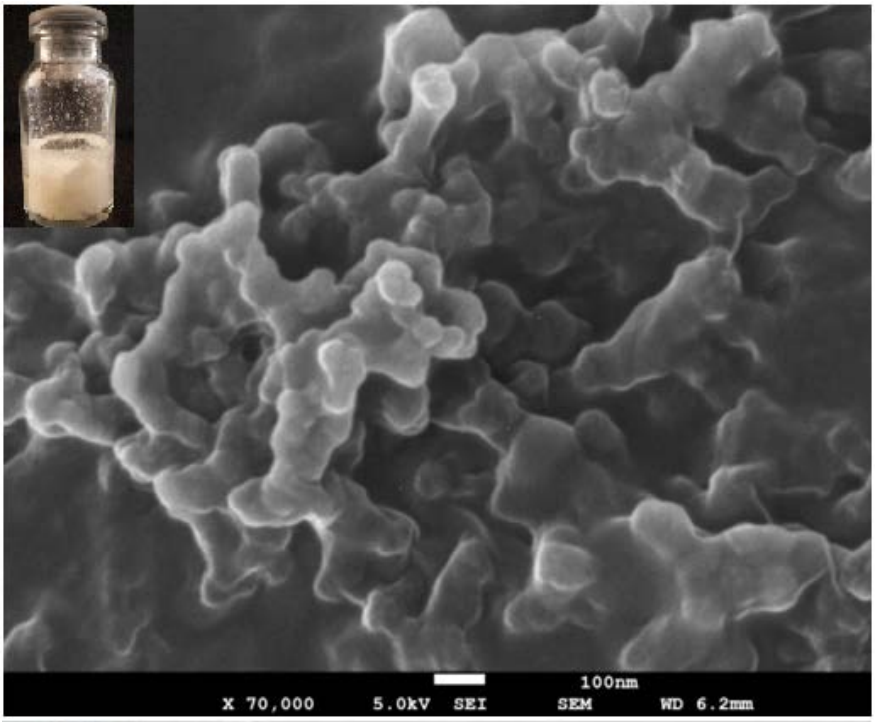
100nm
X 70,000 5.0kV SEI SEM WD 6.2mm

(b)

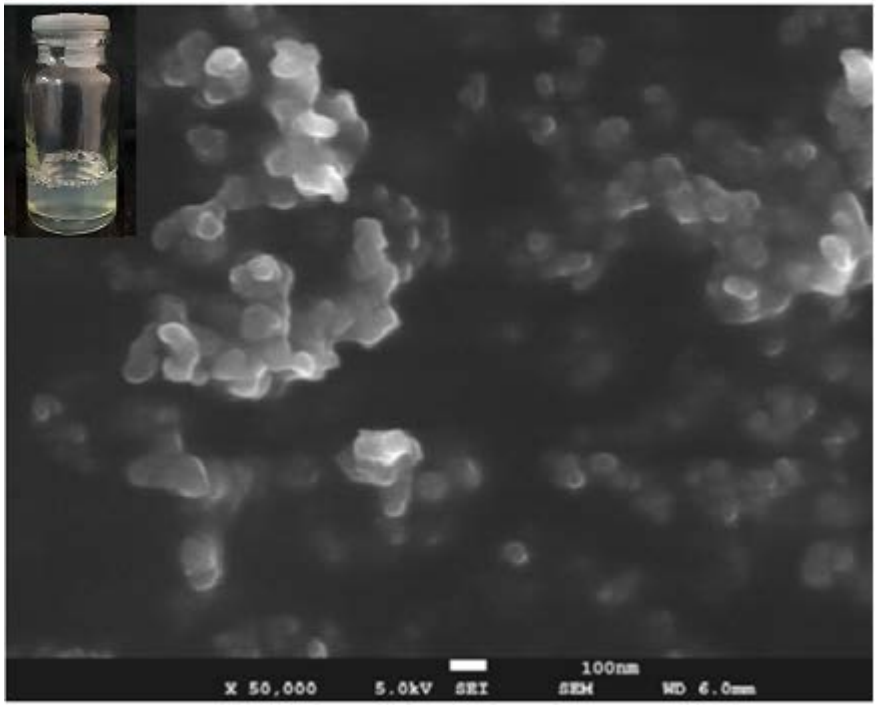
100nm
X 50,000 5.0kV SEI SEM WD 6.0mm

(c)

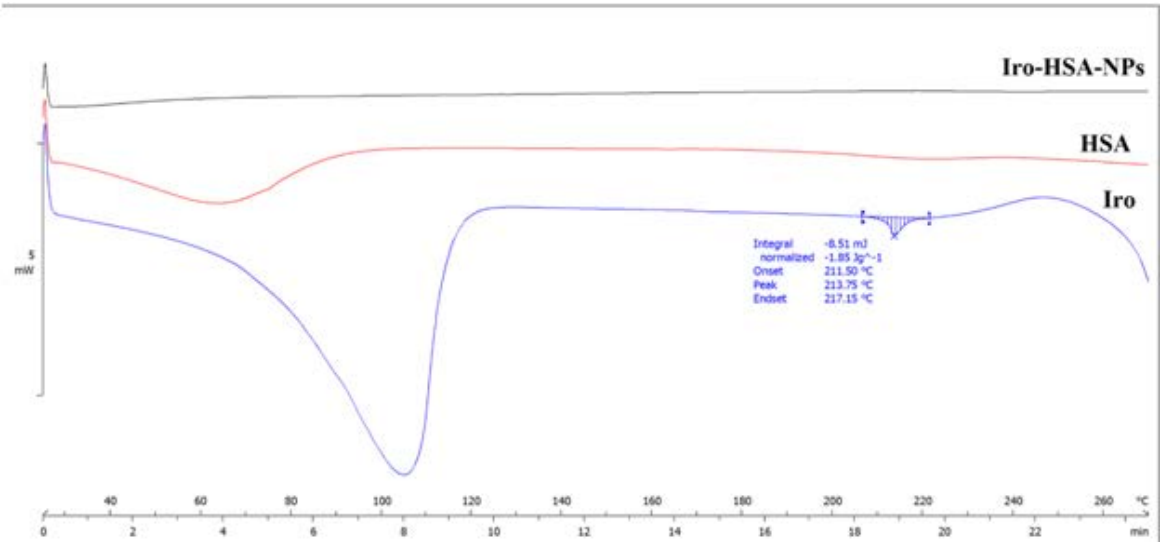
Iro-HSA-NPs
HSA
Iro
Integral -8.51 mJ
normalized -1.85 Jg^-1
Onset 211.50 °C
Peak 213.75 °C
Endset 217.15 °C
5
mW
40 60 80 100 120 140 160 180 200 220 240 260 °C
0 2 4 6 8 10 12 14 16 18 20 22 min

(d)

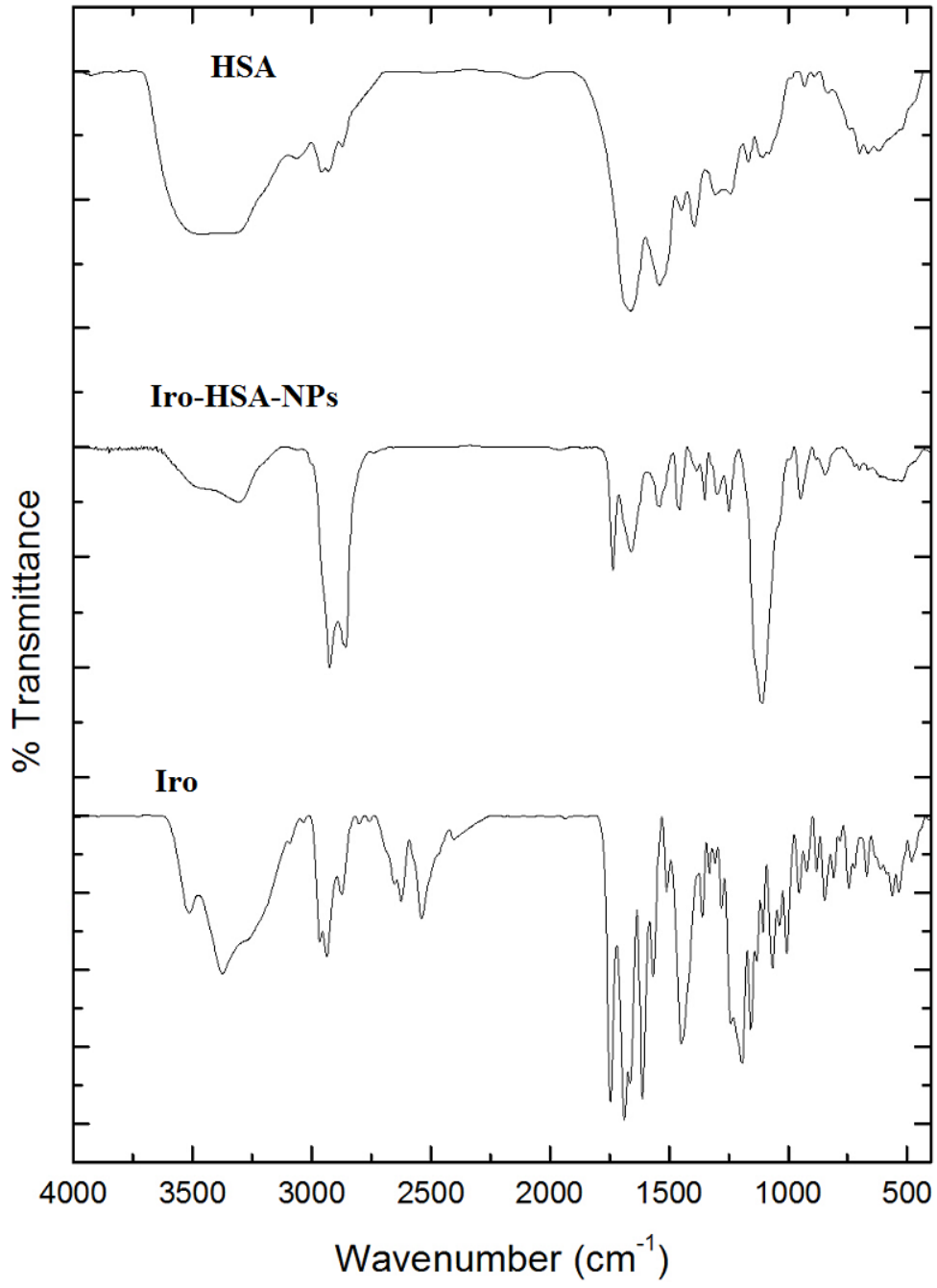
HSA
Iro-HSA-NPs
Iro
% Transmittance
4000 3500 3000 2500 2000 1500 1000 500
Wavenumber (cm-1)

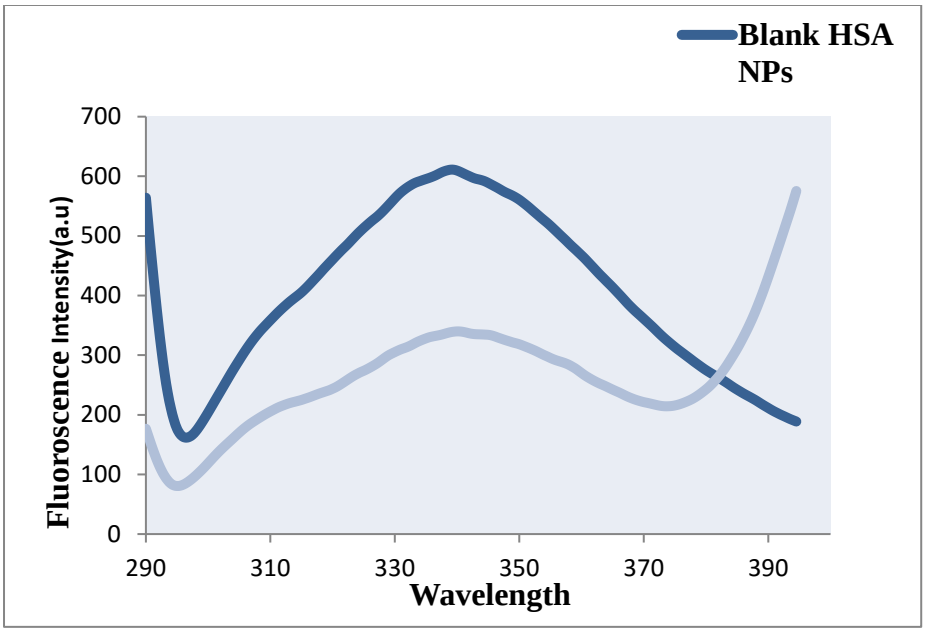

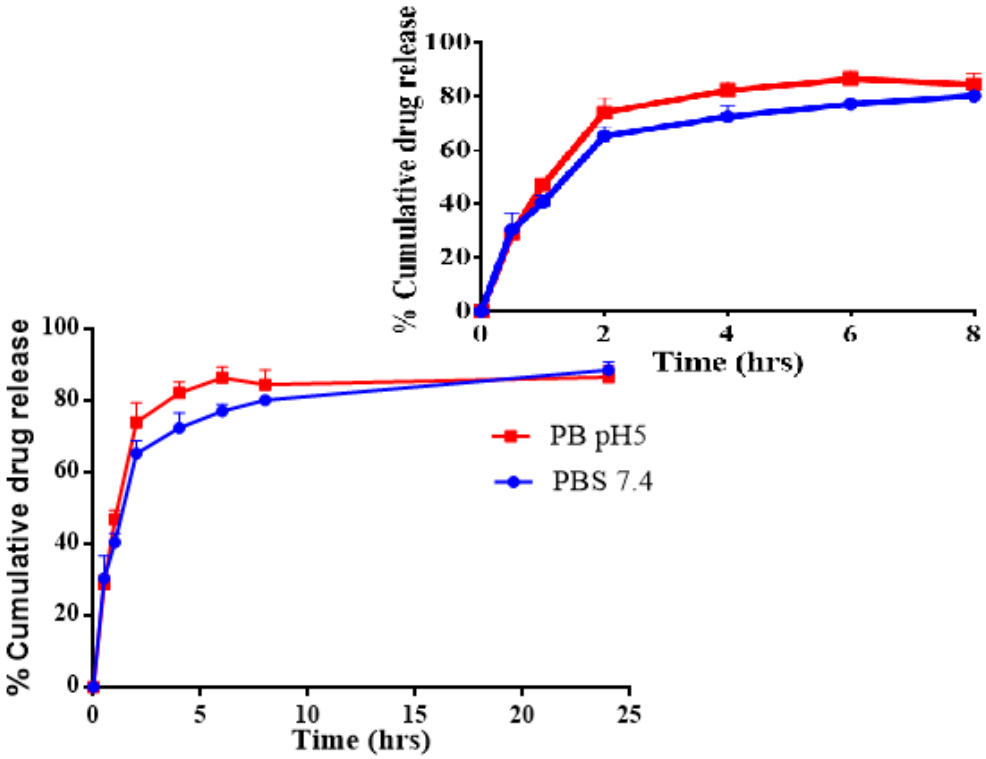

Fig. 6 (a) Surface electron microscopy images of lyophilized Iro-HSA-NPs and (b) after reconstitution of lyophilized NPs (c) DSC thermogram overlay of irinotecan (Iro), Human serum albumin (HSA) and Irinotecan HSA Nanoparticles (Iro-HSA-NPs), (d) FTIR spectra of HSA, Irinotecan and Iro-HSA-NPs, (e) Flouoroscence spectroscopy of Blank and Iro-HSA-NPs and (f) *In-vitro* release of irinotecan from Iro-HSA-NPs in phosphate buffer saline pH 7.4 (PBS 7.4) and Phospahte buffer pH 5 (PB 5) at 37^0 C; Inset *In-vitro* release of irinotecan from Iro-HSA-NPs in phosphate buffer saline pH 7.4 (PBS 7.4) and Phospahte buffer pH 5 (PB 5) at 37^0 C till 8 hours.

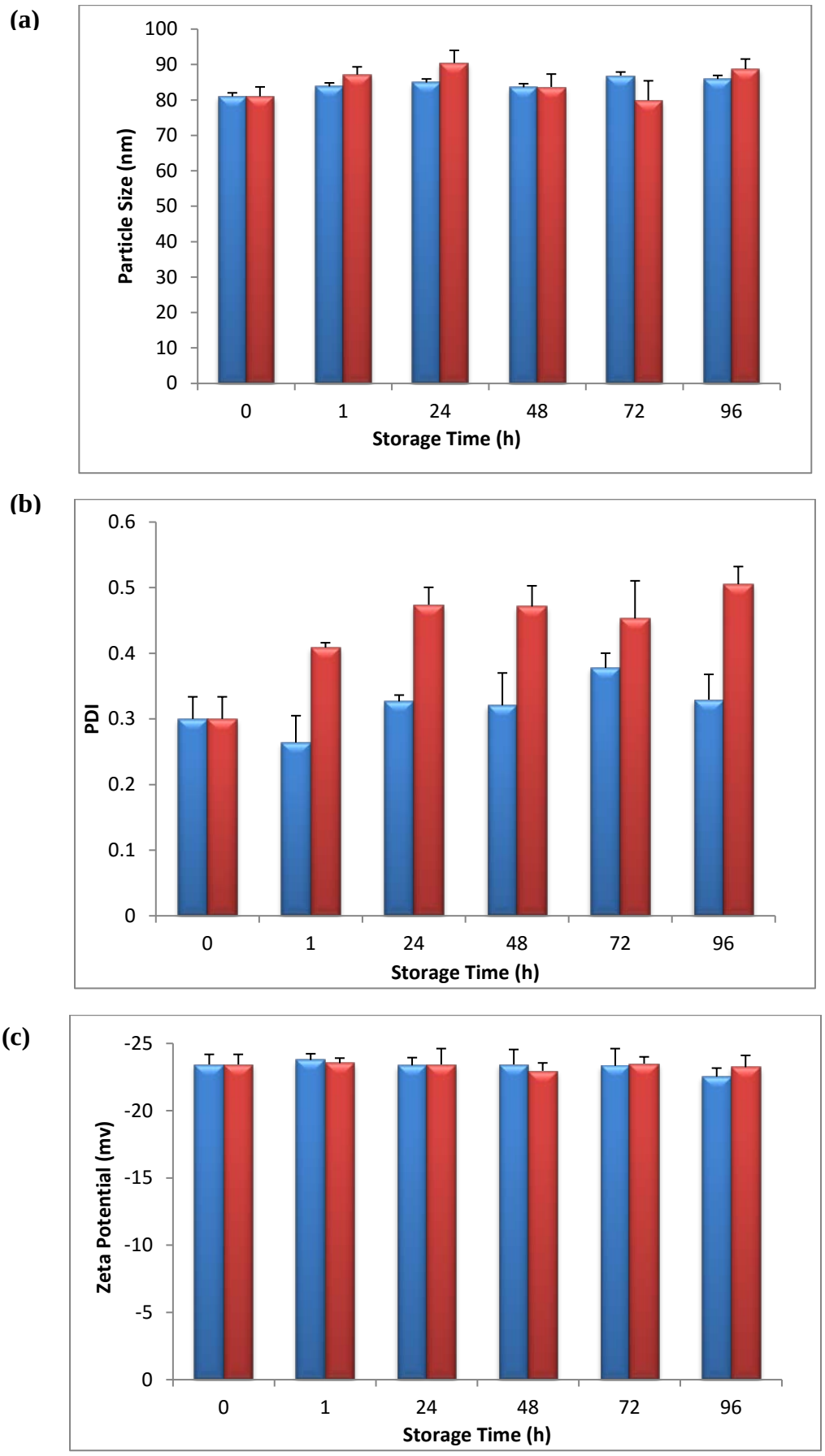

Fig. 7 Short-term stability study of Iro-HSA-NP dispersion; Effect on (a) mean particle size (b) polydispersity index and (c) zeta potential (mV) recorded over a period of 96 hours storage at 4^0C(■) and 25^0C (■).

(a) **(b)**

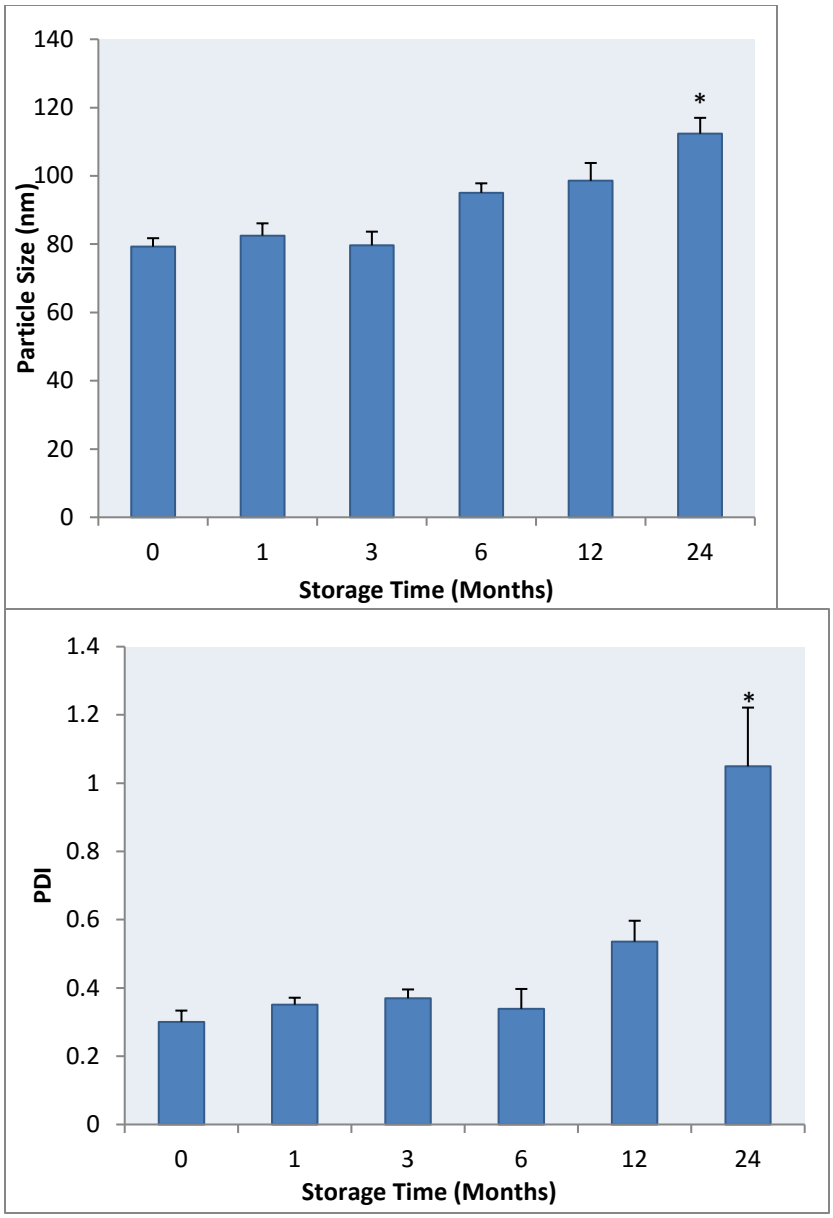
140
120
100
80
60
40
20
0
Particle Size (nm)
*
0
1
3
6
12
24
Storage Time (Months)
1.4
1.2
1
0.8
0.6
0.4
0.2
0
PDI
*
0
1
3
6
12
24
Storage Time (Months)

(c) **(d)**

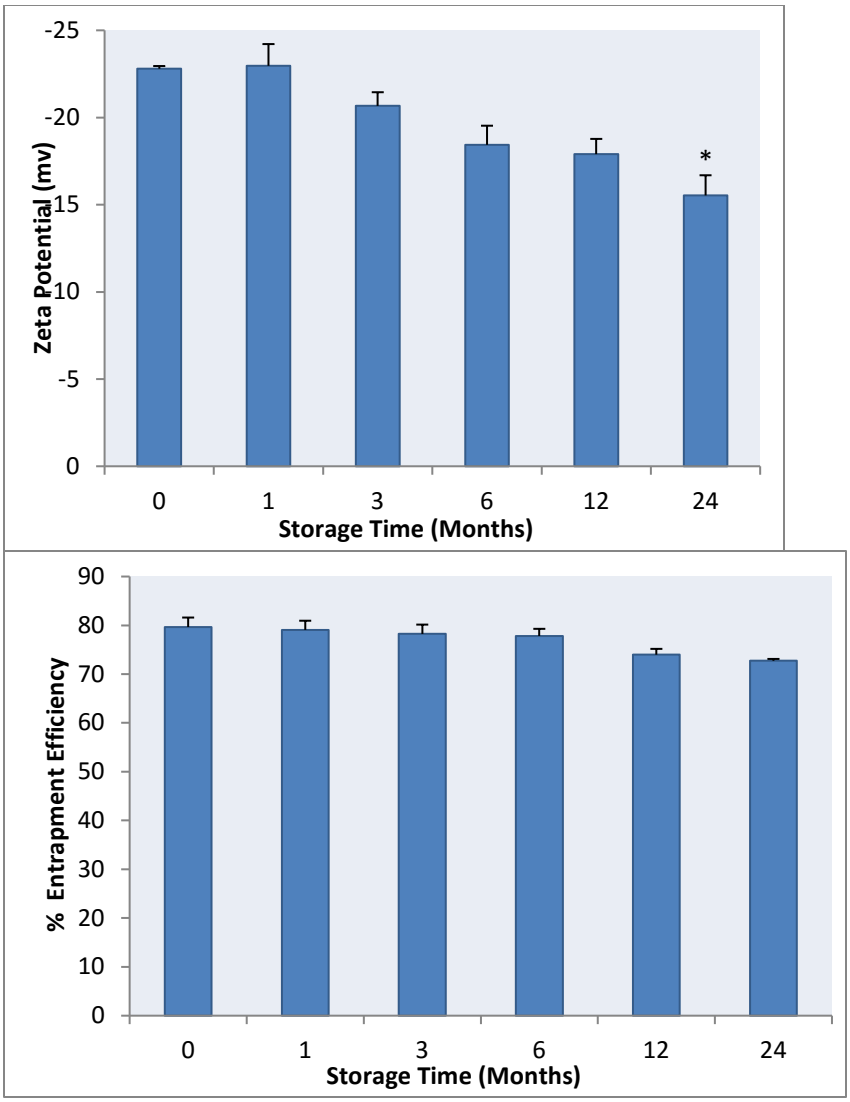

Fig. 8 Long-term stability of freeze dried Iro-HSA-NPs; Effect on (a) Mean particle size (b) Polydispersity index (c) Zeta potential and (d) Entrapment efficiency recorded over period of 24 months storage at 4^0C. The freeze dried samples were reconstituted before analysis.

Table 1: Mean particle size and polydispersity index of Iro-HSA-NPsat different homogenization pressures and number of homogenization cycles

Homogenization Pressure	Homogenization Cycles							
	2		4		6		8	
	MPS	PDI	MPS	PDI	MPS	PDI	MPS	PDI
200	853.3	0.984	500	0.675	350.4	0.582	302.4	0.441
400	231.8	0.321	211	0.432	142.7	0.403	109.3	0.339
600	100.5	0.321	94.9	0.346	81.9	0.21	78.84	0.186
800	105.2	0.491	98.1	0.473	Aggregation	Aggregation	Aggregation	Aggregation

MPS-Mean particle size; PDI-Polydispersity index

Table 2: Input variables and their levels for design of experiments

	Levels		
Input variables	-1	0	+1
X_1=Iro: HSA ratio	1:10	1:20	1:30
X_2 = Crosslinking Temperature (^{0}C)	50	55	60
Response : Particle size (Y_1), Polydispersity Index (Y_2), % Entrapment Efficiency (Y_3) and % Drug Loading (Y_4)			

Iro:Irinotecan; HSA: human serum albumin

Table 3: Statastical analysis results of ANOVA

	Particle Size		PDI		% EE		% DL	
	Coefficient	***p* value**	**Coefficient**	***p* value**	**Coefficient**	***p* value**	**Coefficient**	***p* value**
Constant	71.55		0.19		60.00		5.78	
X_1	0.097	0.8362	0.045	0.1789	9.96	< 0.0001	2.79	0.0001
X_2	1.33	0.0386	0.071	0.05	7.43	< 0.0001	0.87	0.050
X_1X_2	-2.28	0.132	-0.031	0.5664	-0.86	0.0950	0.009	0.9835
X_1^2	3.22	0.010	0.14	0.0232	1.27	0.0520	-0.36	0.5777
X_2^2	6.66	0.0007	-0.065	0.3750	0.56	0.3654	0.95	0.1855

Table 4: Selection and optimization of cryoprotectant for freeze-drying

	Type of Cryoprotectant			
	Mannitol		**Trehalose**	
Cryoprotectant (% w/v)	**Particle size (nm)**	**PDI**	**Particle size (nm)**	**PDI**
0	105.2	0.590	109.8	0.601
2	90.2	0.342	62.8	0.419
4	91.7	0.310	**80.4**	**0.216**
6	72.0	0.290	89.0	0.301

SUPPLEMENTARY FIGURES

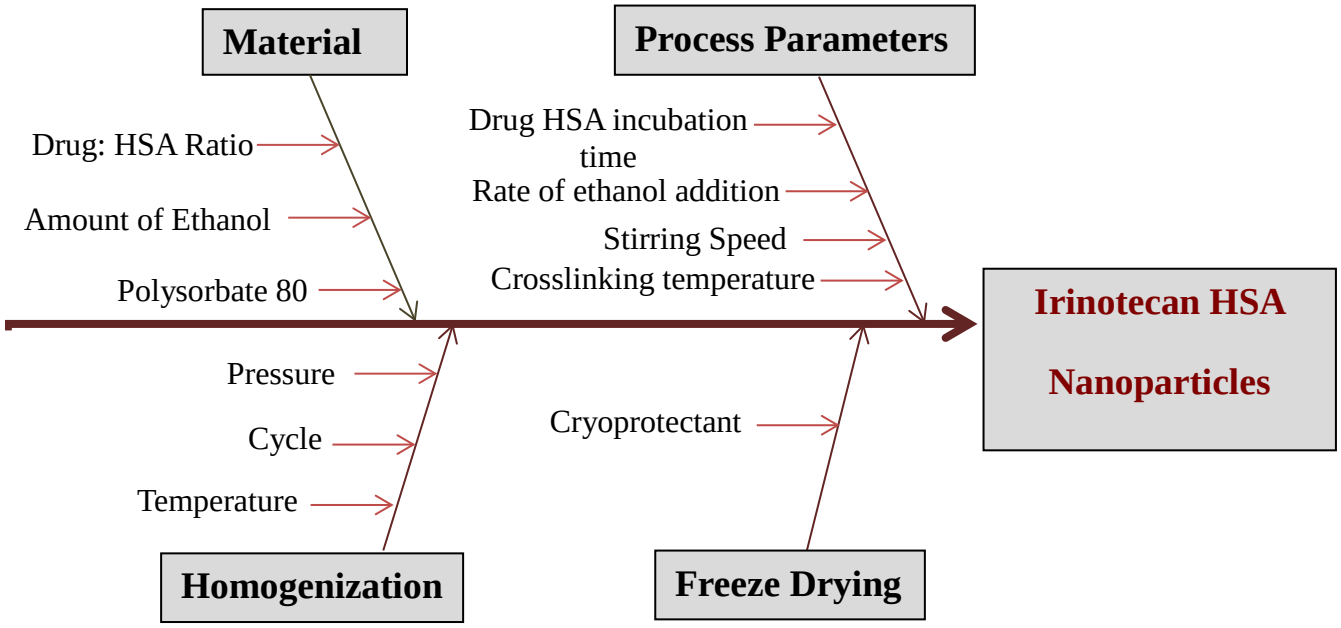

Fig. S1 Ishikawa diagram illustrating product and process variables influencing the critical q

(a)

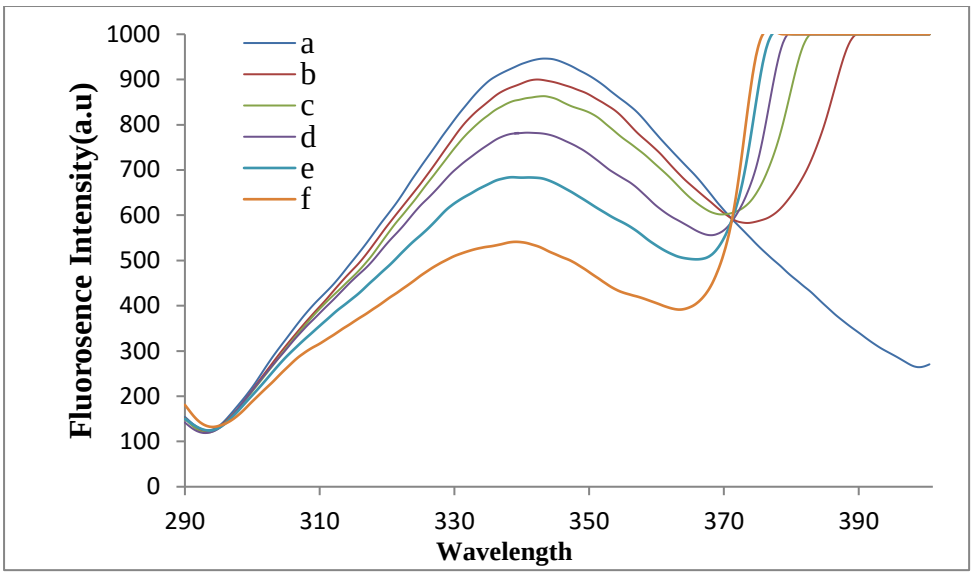

(b)

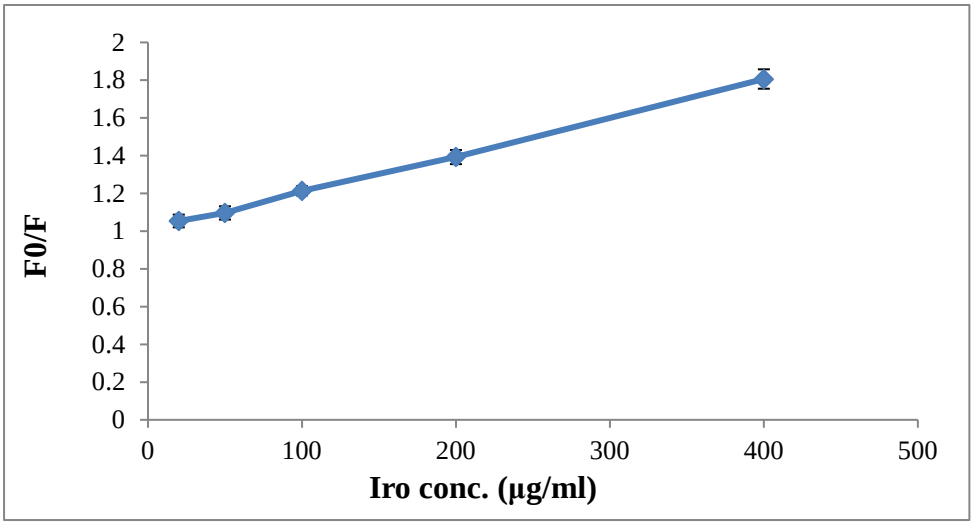

(c)

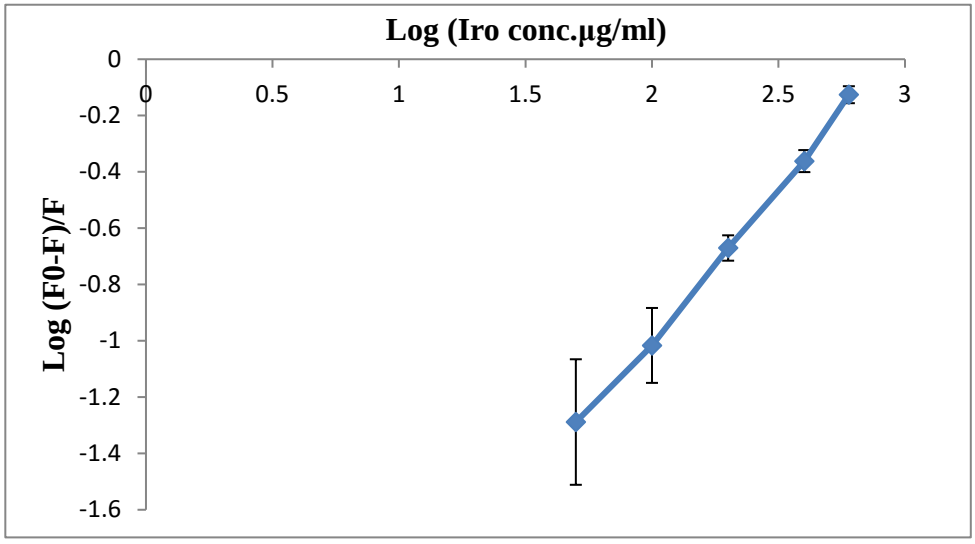

Fig.S2:Binding study of irinotecan and HSA by fluorescence quenching method (a) Fluorescence Spectra (top to bottom) of (a) HSA and (b-f) HSA in the presence of irinotecan in concentration range of 20 µg-400 µg/ml (b) Stern-Volmer plot of F0/F versus Iro for HSA in the presence of different Iro concentration (20-400µg/ml) (c) Binding plot of log (F0-F)/F versus log Iro conc. (20-400µg/ml).

(a)

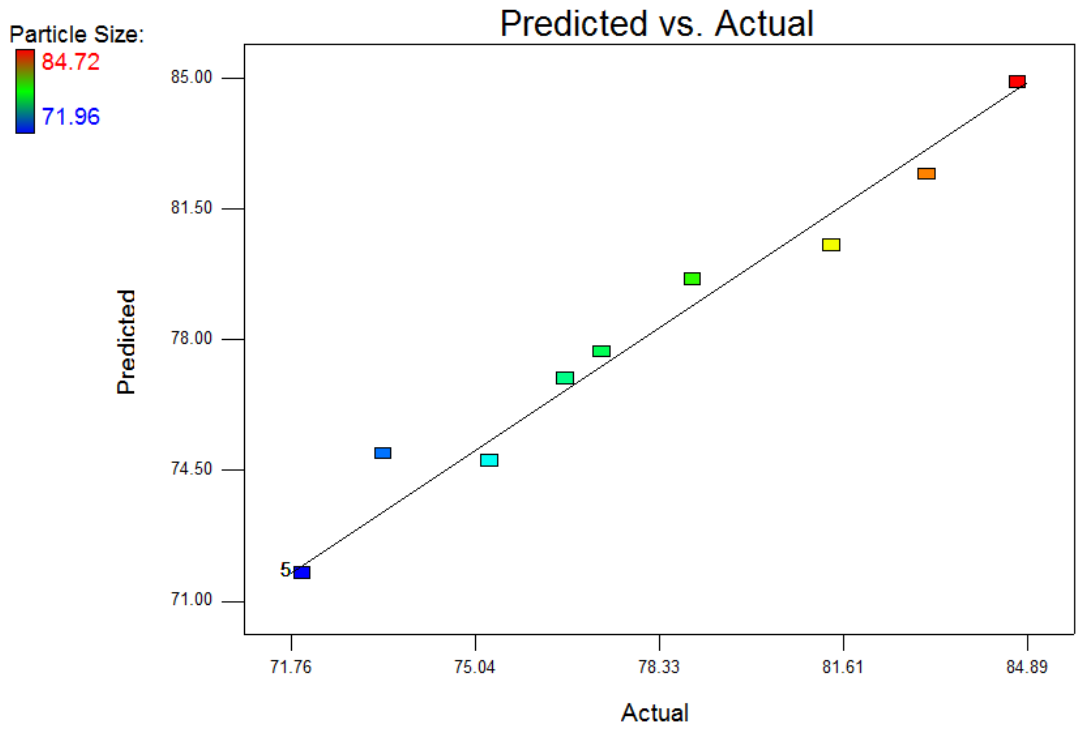
Particle Size:
84.72
71.96
Predicted vs. Actual
Predicted
85.00
81.50
78.00
74.50
71.00
5
71.76
75.04
78.33
81.61
84.89
Actual

(b)

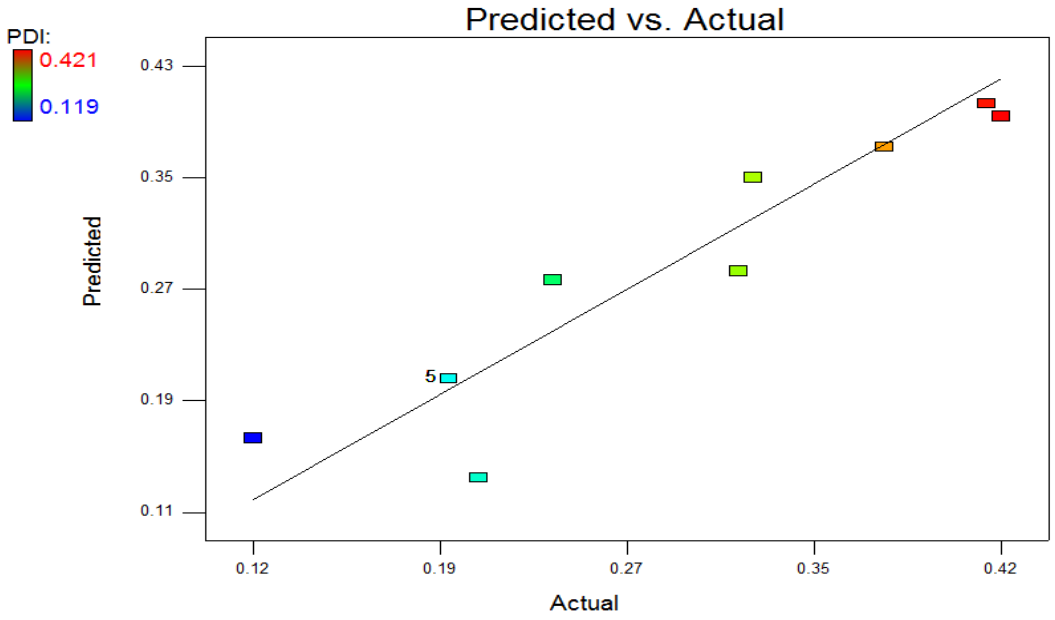
PDI:
0.421
0.119
Predicted vs. Actual
Predicted
0.43
0.35
0.27
0.19
0.11
5
0.12
0.19
0.27
0.35
0.42
Actual

(c)

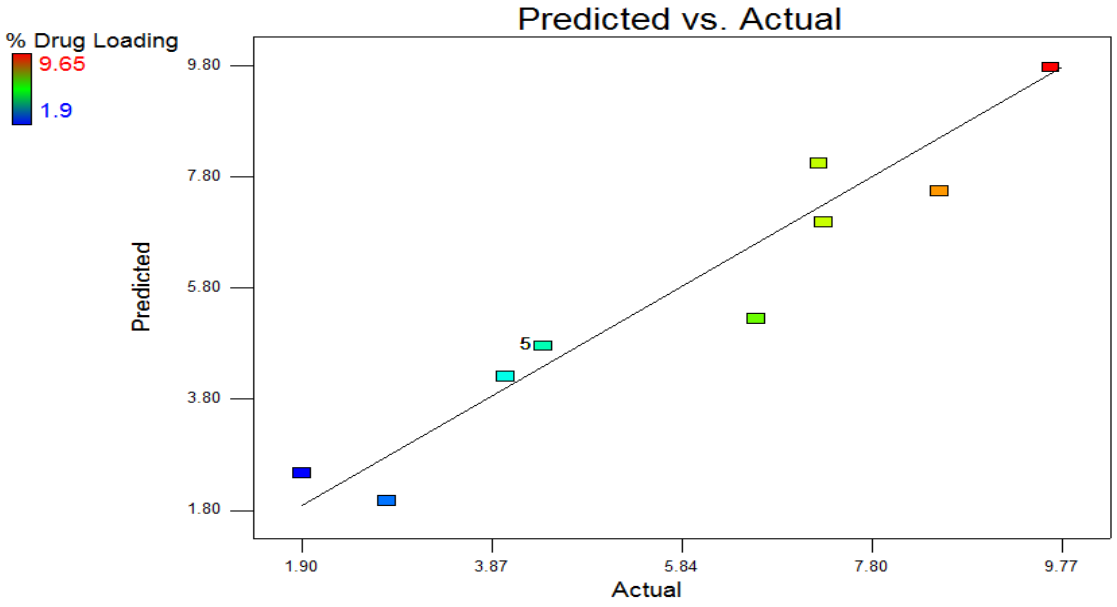

Fig. S3: Predicted vs actual response plot (a) Particle size (b) Polydispersity Index (c) % Entrapment efficiency (d) % Drug Loading

(a)

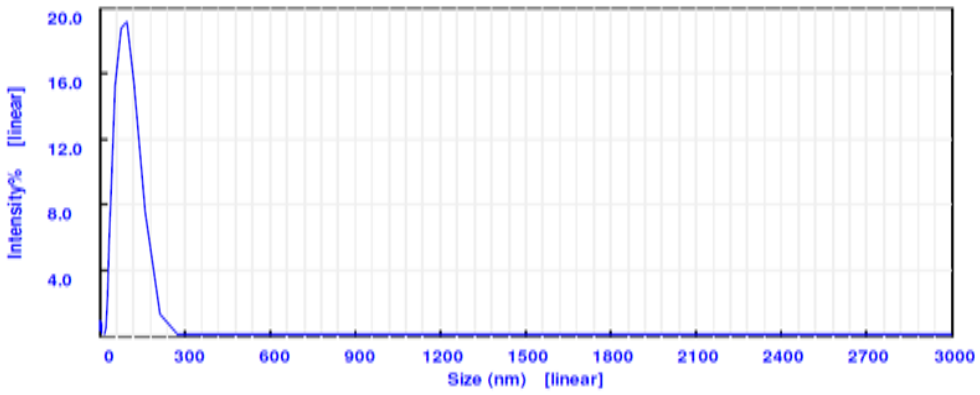

(b)

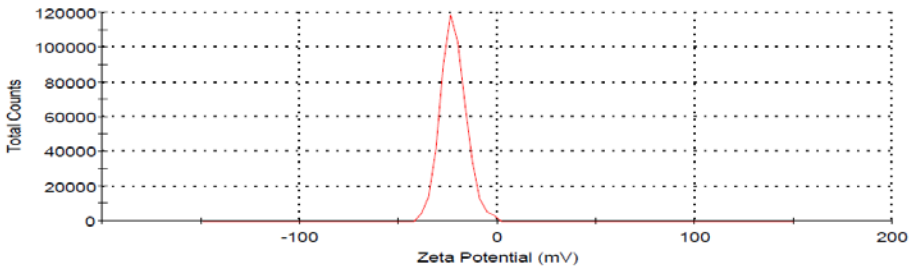

Fig. S4: (a) Particle size distribution of Iro-HSA-NPsby dynamic light scattering spectroscopy (b) Zeta potential of Iro-HSA-

Table S1: Risk assessment matrix for control of critical quality attributes for fabricating Iro-HSA-NPs

Risk assessment related to		Particle Size	Polydispersity Index	Entrapment Efficiency	Drug Loading	Stability
Materials	Iro: HSA Ratio	Medium	Medium	High	High	Low
	Polysorbate 80	Medium	Medium	High	High	High
	Ethanol	High	High	Low	Low	Medium
Process	IroHSA incubation time	Low	Low	High	High	Medium
	Rate of ethanol addition	High	High	Low	Low	Low
	Crosslinking temperature	High	High	High	High	Low
	Stirring speed	High	High	Low	Low	Medium
Homogenization	Temperature	High	High	High	High	Low
	Pressure	High	High	Low	Low	High
	Cycle	Medium	Medium	Medium	Medium	Medium
Freeze Drying	Cryoprotectant	High	High	Low	Low	High

Table S2: Optimization of incubaton time of Irinotecan and human serum albumin solution for preparation of Iro-HSA-NPs

Incubation time (hours)	Appearance of Iro HSA solution
No incubation	Unclear solution with drug precipitates
1	Unclear solution with drug precipitates
2	Hazy solution with no precipitates
3	Clear solution